Petrology of the Alkaline Core of the Messum Igneous Complex, Namibia: Evidence for the Progressively Decreasing Effect of Crustal Contamination

Article *in* Journal of Petrology · September 1999

DOI: 10.1093/petroj/40.9.1377 · Source: OAI

3 authors, including:

Chris Harris
University of Cape Town
310 PUBLICATIONS **7,302** CITATIONS

JOURNAL OF PETROLOGY | VOLUME 40 | NUMBER 9 | PAGES 1377–1397 | 1999

Petrology of the Alkaline Core of the Messum Igneous Complex, Namibia: Evidence for the Progressively Decreasing E ect of Crustal Contamination

CHRIS HARRIS[1]*, JULIAN S. MARSH[2] AND SIMON C. MILNER[3]

[1]DEPARTMENT OF GEOLOGICAL SCIENCES, UNIVERSITY OF CAPE TOWN, RONDEBOSCH 7700, SOUTH AFRICA

[2]DEPARTMENT OF GEOLOGY, RHODES UNIVERSITY, GRAHAMSTOWN 6140, SOUTH AFRICA

[3]GEOLOGICAL SURVEY, P.O. BOX 2168, WINDHOEK, NAMIBIA

RECEIVED NOVEMBER 12, 1998; REVISED TYPESCRIPT ACCEPTED APRIL 12, 1999

The Messum complex of NW Namibia, a part of the Paraná–Etendeka volcanic province, consists of a dominantly felsic central core, surrounded by older gabbros. The igneous rocks of the core can be divided, in order of decreasing age, into (1) a sub-alkaline suite, (2) an outer quartz syenite suite, and (3) an inner silica-undersaturated suite dominated by nepheline syenite. Compositional differences within the quartz syenite suite can be explained by fractional crystallization, but Sr- and O-isotope data indicate that these rocks contain a significant crustal component. The younger central nepheline syenites trend towards the 0·1 GPa phonolite minimum and appear to have evolved by closed system fractional crystallization of a mantle-derived magma, whereas earlier nepheline syenites appear to be contaminated with quartz syenite. The decreasing effects of crustal contamination with time may reflect progressive armouring of the magmatic plumbing system by less contaminated material. Basanite dykes that intrude the plutonic rock of the core show trace element and Nd- and Sr-isotope characteristics that are similar to those of basanites from Tristan da Cunha. This suggests that the mantle-derived component of the Messum core rocks came from the Tristan plume.

KEY WORDS: *Paraná–Etendeka volcanism; Messum complex; alkaline core; crustal contamination; Tristan plume*

INTRODUCTION

The Etendeka Igneous province in the Damaraland region of northwest Namibia (Fig. 1) contains numerous anorogenic igneous complexes of Mesozoic age (Martin *et al.*, 1960; Piranjo, 1994), one of which is the Messum complex. The range in chemical composition, both within and between the various complexes, is remarkable and includes both silica-oversaturated and silica-undersaturated mafic and felsic rocks, including carbonatite. Messum was classified as a 'mixed complex' by Harris (1995), as it contains substantial amounts of both silica-undersaturated and silica-oversaturated rock types.

Dating of several Damaraland complexes yields ages that lie between 137 and 124 Ma (Siedner & Miller, 1968; Milner *et al.*, 1995*b*; Renne *et al.*, 1996). The alignment of the complexes along two parallel NE–SW trends suggests that they represent a hotspot trace caused by the motion of the African plate over a fixed mantle plume (e.g. Rhodes, 1971). Because there is no systematic age progression along the lineament, this view has generally been discounted (Marsh, 1973). Recent ideas that large continental flood basalt (CFB) provinces, such as the Paraná–Etendeka province, are manifestations of mantle plume activity (White & Mackenzie, 1989) has refocused attention on the relationship between plumes and linear arrays of complexes in CFB provinces. Milner *et al.* (1995*b*) have shown that the Damaraland complexes are contemporaneous with the regional Etendeka flood

*Corresponding author. Telephone: +21-650-2926. Fax: +21-650-3783. e-mail: kv@geology.uct.ac.za

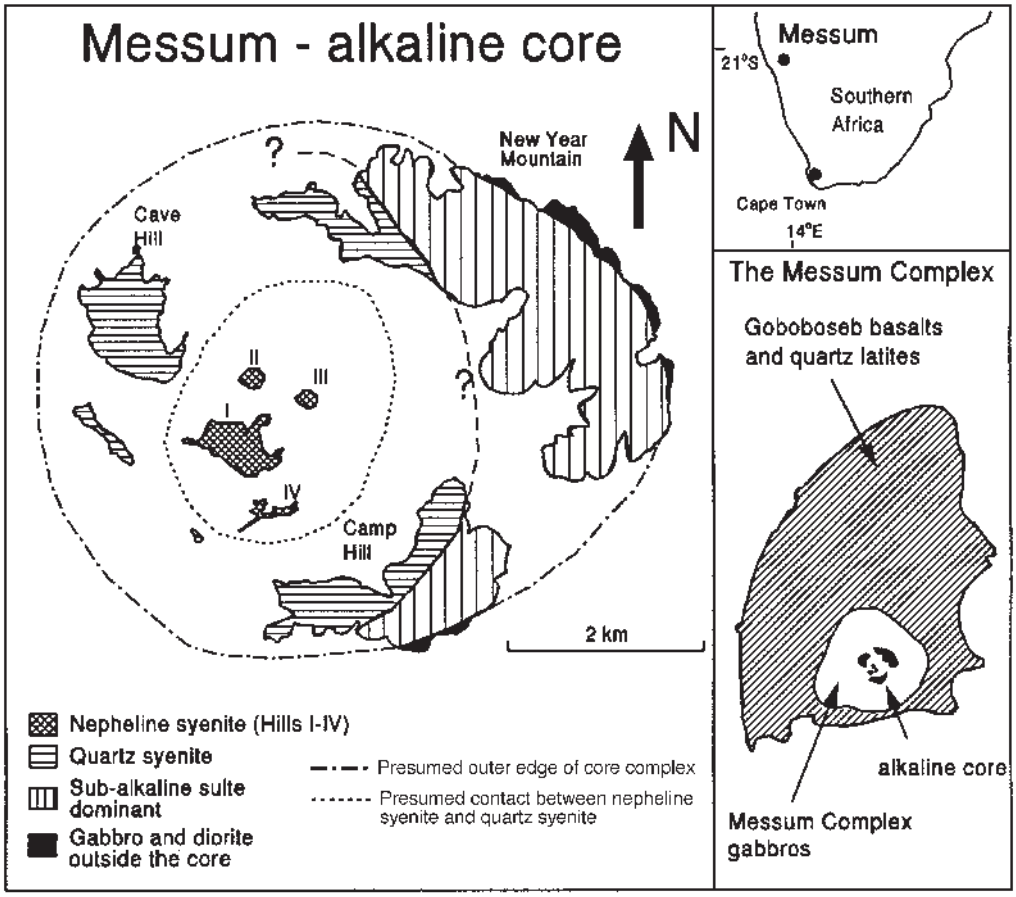

Fig. 1. Geological sketch map of the alkaline core of the Messum complex. The upper right-hand inset shows the location of Messum in southern Africa and the lower inset diagram is a sketch of the relationship of the alkaline core with the outer gabbroic part of the complex and the surrounding Goboboseb volcanic rocks (from Ewart *et al.*, 1998*a*). Within the central nepheline syenite body, there are four prominent hills (labelled I–IV) which may represent discrete intrusions (see text). The flat area occupied by nepheline syenite lies between the hills and the presumed contact between nepheline syenite and quartz syenite.

volcanism and have proposed that all Etendeka igneous activity is a result of a single thermal event related to the upwelling of the Tristan plume during rifting of South America and Africa.

Within this context, our study of the alkaline rocks in the core of the Messum complex addresses two important issues in igneous petrogenesis. Messum is notable for a wide range in the composition of the igneous rocks of both alkaline and tholeiitic parentage that build the complex. Specifically, the close association of quartz- and nepheline-bearing felsic alkaline rocks, and their petrogenetic relationship, a perennial problem in alkaline rock petrology (e.g. Foland *et al.*, 1993), is one question we address in this paper. The other relates to the role of the Tristan plume in the magmatic evolution of individual complexes. Milner & le Roex (1996) have demonstrated the presence of alkaline gabbros having the geochemical characteristics of the modern Tristan plume in one of the Damaraland complexes, Okenyenya. How widespread is this feature in the Damaraland complexes? Mafic alkaline rocks occur in the core of Messum in association with the felsic types and clearly provide the opportunity to investigate this issue.

Previous work

The geology of Messum was first described in detail by Korn & Martin (1954), and they and Mathias (1956, 1957) discussed the petrogenesis of the alkaline rocks of the core of the complex. These workers interpreted the syenitic character of the core as being due to metasomatic transformation of pre-existing volcanic rocks into nepheline syenite and syenite, with only a part of the central core being truly magmatic. Mathias (1956) argued that some of the granitic rocks were magmatic and some were metasomatic, the two types being gradational, and considered the evidence for a magmatic as opposed to a

metasomatic origin for the nepheline syenite central core to be equivocal. However, both sets of workers considered the theralites (nepheline-bearing gabbro) to be metasomatized gabbros of the same composition as the outer tholeiitic gabbros. Such large-scale 'transformationist' petrology is no longer in vogue as a modern petrogenetic interpretation. However, the possibility remains that at least some of the silica-undersaturated rocks in the poorly exposed area between the central nepheline syenite plugs and the major masses of quartz syenite are partly of metasomatic origin, in that they could represent fenitized quartz syenite.

GEOLOGY OF MESSUM

The Messum complex is roughly 18 km in diameter and consists of a diverse assemblage of intrusive and extrusive phases, which intrude the volcanic sequence of the Goboboseb Mountains. Although the latter forms a collar around Messum, there is no strong evidence for a petrogenetic link between the volcanic rocks immediately surrounding the complex and the preserved rocks of the complex. However, Messum is important in the evolution of the Paraná–Etendeka province, as it is the eruption centre for some of the very large-volume quartz latite sheets found in the regional volcanic sequence in the Etendeka and the SE Paraná in Brazil (Milner & Ewart, 1989; Milner *et al.*, 1995*a*). The outline of the complex is roughly circular, and in most places the outer contacts are covered by sand (Ewart *et al.*, 1998*a*). The rocks of the complex can be divided into an outer series of gabbro and granite cone sheets and an inner core complex of syenites, nepheline syenites and volcanic breccia. There are also basalts, which occur within the complex itself (the Messum Crater Basalts, Ewart *et al.*, 1998*a*) and have no compositional equivalents outside the complex.

The outer series of gabbros can be divided into two separate sets of cone sheets, which dip towards the centre of the complex (Korn & Martin, 1954; Ewart *et al.*, 1998*a*). The western cone sheets form two semi-circular rings, which consist of anorthosite, troctolite, olivine gabbro and gabbro, all of which are cut by dykes and sills of microgabbro. This sequence has been interpreted as two thick cumulate sequences (900–2425 m total thickness) possibly in the form of interconnected cone sheets that are dominantly inward dipping with the outer ring averaging 38° and the inner ring 52°. These cone sheets are cut by numerous granitic sheets, which show physical evidence for hybridization and mixing along the contact between the gabbros and the granites. The eastern gabbros consist of thinner sheets, which dip at a shallower angle (average of 25°), towards the centre of the complex. They are dominantly gabbro–norite containing visible biotite in hand specimen: this distinguishes them from the western gabbros, which are biotite free. The eastern gabbros intruded what appears to be an older cone sheet complex of heterogeneous granitoid, but there is evidence of commingling of the felsic and gabbroic magma types. Two gabbros and a quartz diorite from the outer part of the complex have been dated using the $^{40}Ar/^{39}Ar$ method (Renne *et al.*, 1996) and yield statistically indistiguishable ages between 131·7 ± 0·7 and 132·1 ± 1·2 Ma. These ages are similar to those obtained by Renne *et al.* (1996) for the Etendeka lavas (131·9 ± 0·6 to 132·3 ± 0·4 Ma) using the same method.

The central region of the complex ('the core') is some 6 km in diameter (Fig. 1). The following three suites of rocks are identified as building the core: (1) silica-undersaturated suite; (2) quartz syenite suite; (3) subalkaline (breccia) suite. These are illustrated on a total alkali–silica (TAS) plot (Fig. 2). The silica-undersaturated suite is largely confined to the central part of the core. Here, nepheline syenites are cut by dykes of a wide range of silica-undersaturated compositions. Associated with the nepheline syenites are a number of nepheline-bearing gabbros (theralites). The silica-undersaturated suite has a continuous range in composition from nepheline gabbro–basanite through to phonolite (Fig. 2). Within this suite, we recognize the following rock types: nepheline syenites, theralites, and dykes that cut the core rocks. Amongst the least-evolved nepheline syenites are four samples (MC4, MC44, MC42, MC43) that frequently plot well away from other samples and are discussed separately below.

The nepheline syenite in the core may be a series of intrusions rather than a single body. Four small hills in this central core area (Fig. 1) may represent distinct nepheline syenite intrusions, albeit of similar or identical age. Evidence of concentric layering and lamination around the base of one of these hills (Mathias, 1956; this work) supports this idea. There is generally little outcrop in the flat areas between the hills, but where outcrop is visible, the nepheline syenite appears to be coarser grained and somewhat poorer in nepheline than are the rocks building the hills. If the nepheline syenite hills are separate intrusions, then the flat areas must be underlain by an earlier nepheline syenite intrusion(s). Within each hill-forming nepheline syenite intrusion, felsic and mafic facies were found to be present; these show no obvious pattern of distribution. They were not mapped in detail because of the difficulty in distinguishing between types on weathered surfaces, and the apparent absence of systematic facies change. The theralite bodies are found as a series of lenticular pods with obscure contact relationships with the nepheline syenite. It was not possible to ascertain if one was intrusive into the other, though it seems most likely that the theralites intruded the nepheline syenites. Milner *et al.* (1995*b*) obtained a Rb–Sr internal isochron age of 126·8 ± 1·3 Ma from a single

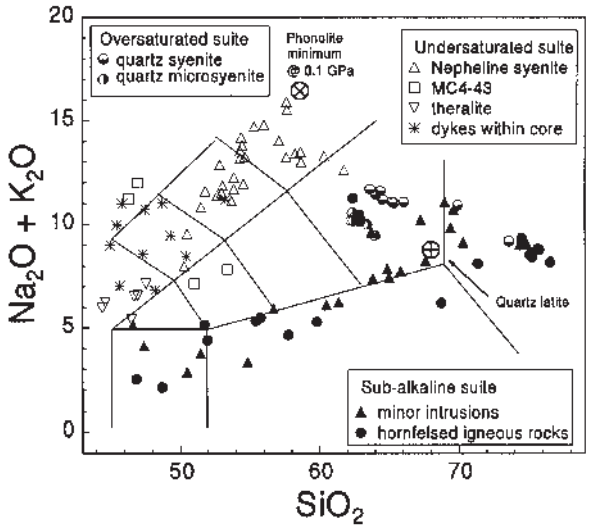

Fig. 2. Total alkali–silica (TAS) diagram with Messum core whole-rock compositions plotted. The three main suites are indicated as (silica) oversaturated, (silica) undersaturated and subalkaline. It should be noted that the group of minor intrusions in the subalkaline suite intrude the breccia complex and do not intrude the alkaline rocks of the core. The boundaries for di erent rock types of Le Maitre *et al.* (1989) are indicated. The average composition of quartz latite units I and II that were erupted from Messum (Ewart *et al.*, 1998*b*) is plotted and the 0·1 GPa phonolite minimum in the system quartz–nepheline–kalsilite–water (Schairer, 1950) is indicated.

sample of nepheline syenite (MC4), and Renne *et al.* (1996) obtained a $^{40}Ar/^{39}Ar$ age of 129·3 ± 0·7 Ma on hornblende also from a nepheline syenite. The cause of the discrepency in age is not known. These results indicate that the alkaline rocks are younger than the Messum tholeiitic rocks, and that in the context of the regional evolution of the volcanic province, the silica-undersaturated alkaline igneous activity at Messum was a late-stage phenomenon.

The quartz syenite suite surrounds the nepheline syenites (Fig. 1) and consists of syenite and quartz microsyenite ranging in SiO_2 content up to granite composition (Fig. 2). This suite has no mafic components. The quartz syenites are extremely heterogeneous on a variety of scales, and in places contain a high proportion of enclaves. The amount of quartz in the syenites is variable, ranging from a fraction of a percent, up to 10–15% in rocks that should more properly be called granites. The quartz syenites are intruded by silica-undersaturated dykes and are interpreted to be older than the nepheline syenites.

The sub-alkaline (breccia) suite forms an incomplete ring around the eastern margin of the core and builds the most prominent peaks of the core, including the bulk of New Year Mountain. These rocks are a chaotic mixture of hornfelsed volcanic, fine-grained intrusive, and sedimentary rocks. Volcanic rocks dominate and include lava flows, fragments of lava flows and a variety of volcaniclastic rocks. Sedimentary rocks include indurated talus slope breccias as well as some minor lake deposits. Clasts within the volcaniclastic rocks and talus breccias are dominated by subaerially erupted volcanic material, and the lake deposits are, in part, composed of remarkably pure, well-sorted quartz arenite. Analyses of lavas and igneous clasts indicate that they are subalkaline in nature and range in composition from basalt to rhyolite (Fig. 2). Along the inner (western) margin the breccia complex is underlain and intruded by sheets of the quartz syenite suite. Numerous anastomosing bodies of a petrographically distinctive feldspar-phyric quartz microsyenite intrude both the breccias and the quartz syenites. This quartz microsyenite is compositionally similar to the coarse-grained quartz syenites described above.

The sub-alkaline suite is regarded as a fragment of the subaerial volcanic superstructure built during an earlier subalkaline phase in the evolution of the Messum volcano. This suite of rocks appears to have collapsed along a caldera margin and been partially engulfed in the rising syenitic magma. These rocks are not considered further in any detail in this paper, which focuses on the magmatic syenite and nepheline syenites.

In summary, the sequence of events that took place during the formation of the Messum Complex is as follows. The Messum gabbros and spatially associated granitoid sheets pre-date the alkaline rocks of the core. They were intruded by quartz syenites and this event was accompanied by collapse of a large fragment of the superstructure of the Messum volcano. Then followed the intrusion of the silica-undersaturated magmas comprising a suite of nepheline syenites and associated theralites followed by late-stage basanitic dykes.

ANALYTICAL METHODS

All major and trace element (except REE) data on whole rocks were obtained by standard X-ray fluorescence spectrometry (XRF) methods at the University of Cape Town (UCT) and Rhodes University. Details of XRF procedure and estimates of detection limits and precision have been given by Duncan *et al.* (1984) and le Roex (1985). All other data were obtained at UCT. Whole-rock REE abundances were determined by inductively coupled plasma mass spectrometry (ICP-MS) with most errors <2% relative. Analyses of minerals were obtained using a Cameca Camebax wavelength-dispersive electron microprobe. Most of the oxygen isotope data were previously reported by Harris (1995), and new data were produced using the same analytical procedures. The Sr- and Nd-isotope data were obtained following conventional ion-exchange separation using a VG sector multi-collector mass spectrometer in dynamic mode. To correct for mass fractionation e ects, measured $^{87}Sr/^{86}Sr$

and $^{143}Nd/^{144}Nd$ ratios were normalized such that $^{86}Sr/^{88}Sr = 0{\cdot}1194$ and $^{146}Nd/^{144}Nd = 0{\cdot}7219$, respectively. Three analyses of NBS987 made during the course of this work gave $^{87}Sr/^{86}Sr$ ratios of 0·710239(10), 0·710279(11) and 0·710239(9) where the figures in parentheses are the standard errors for repeated measurements of the isotope ratio and relate to the least significant digit(s). Repeated analyses of La Jolla Nd at UCT gave a value for $^{143}Nd/^{144}Nd$ of 0·511820. Rb and Sr were determined by XRF and for the three samples with <100 ppm Sr (MC74, MC76 and MC83), longer counting times were employed. The error on Sr for these samples based on counting statistics is 0·58 ppm (2σ). The uncertainty in the age and in the Rb/Sr ratios has no significant e ect on calculated initial ratios, except in the case of the aforementioned samples. These errors are discussed in the modelling section.

PETROGRAPHY AND MINERAL CHEMISTRY

Nepheline syenites

These rocks range from nepheline monzonite to true nepheline syenite and also include nepheline-bearing syenites, some of which contain only a trace of nepheline. For convenience they will be referred to collectively as nepheline syenite. They are medium- to fine-grained equigranular to slightly porphyritic with larger primocrysts of alkali feldspar, nepheline and more rarely clinopyroxene. In some rocks, a strong fabric is developed, which is defined by elongate ferromagnesian minerals and alkali feldspar. Nepheline and alkali feldspar are the dominant minerals in most of these rocks, but a minority contain subordinate plagioclase. The ferromagnesian minerals include clinopyroxene, amphibole and biotite. Sodalite, opaque oxides and apatite are ubiquitous accessory minerals. Amphibole is generally more common than pyroxene; the pyroxenes usually have colourless cores and green rims, and are sometimes surrounded by amphibole. Biotite is generally found as minor replacement patches in amphibole and pyroxene, or as rims around opaque oxides.

The group of four samples (MC4, MC42, MC43 and MC44) are distinct from the nepheline syenites in that they contain a greater proportion of augite relative to amphibole and contain plagioclase as well as alkali feldspar and nepheline. Samples MC4 and MC44 were collected from near the base of nepheline syenite intrusions (hills) III and I, respectively (Fig. 1). They are both coarse grained and are petrographically similar, containing sodian augite surrounded by amphibole and minor biotite. Nepheline, plagioclase and alkali feldspar constitute about 70% by volume of the rock. Samples MC42 and MC43 are from the same outcrop of fine-grained nepheline syenite on the flanks of hill I, the former being a homogeneous dark rock, the latter having light spots. In thin section these rocks are seen to contain titanaugite, amphibole and minor olivine phenocrysts set in a groundmass of alkali feldspar, nepheline, and acicular amphibole and sodic pyroxene. The light spots in MC43 are up to 6 mm diameter sub-spherical cavities infilled with calcite and a low-relief isotropic mineral (analcite?), which appear to be primary in origin.

Theralites

The theralites [synonymous with nepheline gabbro of Le Maitre *et al.* (1989)] are medium-grained rocks with maximum grain diameter of about 6 mm, which consist of up to about 50% phenocrysts of augite and olivine in the proportions 70:30. The augites show complex zoning and are patchily replaced by biotite. Plagioclase and minor alkali feldspar make up a fairly coarse-grained groundmass and large (up to 6 mm diameter) poikilitic nephelines are present. Opaque oxides are ubiquitous accessory minerals, but amphibole is absent.

Dykes

The dykes can be divided into (1) fine-grained versions of the nepheline syenites, and (2) basanites and phonotephrites. The first group, termed 'tinguites' by Korn & Martin (1954), range from rocks that are texturally similar to the nepheline syenites to finer-grained rocks with a strong igneous lamination. The second group generally contain titanaugite and minor olivine phenocrysts, with a fine-grained groundmass of feldspar, pyroxene and brown amphibole.

Quartz syenites

The quartz syenites contain perthitic alkali feldspar, ranging in size up to 5 mm diameter, with fayalite, aegirine–augite, quartz and amphibole occupying the interstices between amphibole grains. Either amphibole or minor biotite rims the fayalite and in some cases, the amphiboles have cores of colourless augitic pyroxene. The microsyenite contains sparse phenocrysts of zoned sodic plagioclase with thin mantles of alkali feldspar and occasionally phenocrysts of augite. The groundmass contains alkali feldspar, augite mantled by green amphibole, and interstitial quartz.

Mineral chemistry

Microprobe analyses have been made of the constituent minerals of 12 samples from the rocks described above.

Table 1: Selected analyses of minerals

	1	2	3	4	5	6	7	8	9	10	11	12	13	14	15	16	17
SiO_2	65·88	51·52	60·18	49·93	29·55	40·32	38·55	35·54	47·37	47·99	47·83	45·06	50·12	49·48	44·49	37·28	39·04
TiO_2					0·00	0·00	0·00	0·00	0·10	1·24	1·06	1·74	0·36	0·48	1·27	3·22	3·53
Al_2O_3	19·47	29·79	24·36	31·50	0·00	0·10	0·00	0·00	0·20	5·21	6·43	9·64	0·91	1·90	4·18	16·94	12·00
Fe_2O_3									4·59	4·93	3·92	3·49	19·12	6·44			
FeO	0·13	0·30	0·18	0·00	65·02	12·95	18·47	39·90	23·46	2·89	2·67	3·01	9·55	12·38	31·67	14·31	20·20
MnO					4·42	0·00	0·29	1·28	1·80	0·23	0·13	0·00	1·50	0·98	1·29	0·27	0·55
MgO					1·09	46·38	41·23	25·19	2·07	13·02	13·77	12·47	1·14	6·13	3·33	10·05	7·98
CaO	0·86	12·86	6·29	14·71	0·10	0·28	0·41	0·12	18·95	23·11	22·98	23·14	10·52	21·09	8·94	11·60	11·32
Na_2O	6·77	3·62	7·49	2·99					0·75	0·57	0·43	0·31	7·09	1·78	2·22	2·48	2·84
K_2O	6·03	0·18	0·64	0·06					0·00	0·00	0·00	0·00	0·00	0·00	0·98	1·41	1·63
Total	99·14	98·27	99·14	99·19	100·18	100·40	98·95	102·03	99·29	99·19	99·22	98·86	100·32	100·67	98·37	97·56	99·09
Oxygen	8·00	8·00	8·00	8·00	4·00	4·00	4·00	4·00	6·00	6·00	6·00	6·00	6·00	6·00	23·00	23·00	23·00
Si	2·97	2·38	2·71	2·30	0·99	1·00	1·00	0·99	1·95	1·80	1·78	1·69	1·97	1·92	7·15	5·63	6·00
Ti					0·00	0·00	0·00	0·00	0·00	0·04	0·03	0·05	0·01	0·01	0·15	0·36	0·41
Al	1·03	1·62	1·29	1·71	0·00	0·00	0·00	0·00	0·01	0·23	0·28	0·43	0·04	0·09	0·79	3·02	2·17
Fe^3									0·14	0·14	0·11	0·10	0·57	0·19			
Fe^2	0·01	0·01	0·01	0·00	1·83	0·27	0·40	0·93	0·81	0·09	0·08	0·09	0·31	0·40	4·26	1·81	2·59
Mn					0·13	0·00	0·01	0·03	0·06	0·01	0·00	0·00	0·05	0·03	0·18	0·03	0·07
Mg					0·06	1·72	1·59	1·05	0·13	0·73	0·76	0·70	0·07	0·35	0·80	2·26	1·83
Ca	0·04	0·64	0·30	0·73	0·00	0·01	0·01	0·00	0·84	0·93	0·92	0·93	0·44	0·88	1·54	1·88	1·86
Na	0·59	0·32	0·65	0·27					0·06	0·04	0·03	0·02	0·54	0·13	0·69	0·73	0·85
K	0·35	0·01	0·04	0·00					0·00	0·00	0·00	0·00	0·00	0·00	0·20	0·27	0·32
Sum	4·98	4·98	4·99	5·00	3·01	3·00	3·01	3·01	4·00	4·00	4·00	4·00	4·00	4·00	15·75	15·99	16·10

1, MC33 (dyke) alkali feldspar phenocryst; 2, MC3 (theralite) plagioclase; 3, MC4 (ne syenite) plagioclase; 4, MC44 (ne syenite) plagioclase; 5, MC83 (quartz syenite) olivine; 6, MC37 (dyke) olivine; 7, MC18 (dyke) olivine; 8, MC3 (theralite) olivine; 9, MC83 (syenite) pyroxene; 10, MC37 (dyke) pyroxene; 11, MC18 (dyke) pyroxene; 12, MC3 (theralite) pyroxene; 13, MC27 (dyke) pyroxene; 14, MC24 (ne syenite) pyroxene; 15, MC83 (quartz syenite) amphibole; 16, MC18 (dyke) amphibole; 17, MC33 (dyke) amphibole. Space indicates not analysed. Fe^{2+}/Fe^{3+} ratio in pyroxenes calculated using the method of Droop (1987). Amphibole analyses reported with total Fe as Fe^{2+}.

Alkali feldspar in the evolved rocks was analysed only where fresh unexsolved material was present. This excluded feldspars from most of the nepheline syenite samples. Olivine and biotite were present only in a minority of the samples selected for microprobe analysis.

Olivine

Olivine was analysed in two dyke samples (MC37, MC18) and one sample of theralite (MC3) (Table 1; Fig. 3). The basanite dykes have Mg-rich olivine ($Fo_{78–88}$) whereas the theralite sample has more iron-rich olivine ($Fo_{56–47}$). In the one quartz syenite sample analysed (MC83), the olivine surrounded by amphibole and biotite overgrowths is almost pure fayalite (Fo_3).

Clinopyroxene

Because of the high aluminium content of many of the pyroxenes, they are not easily represented on the conventional pyroxene quadrilateral. Figure 3 shows pyroxene compositions plotted on Ac–(Di + Hd)–Ca Tschermak and Na–Mg–(Fe^{2+} + Mn) triangular diagrams, which illustrate best the compositional range [where Ca Tschermak component includes $CaAl_2Si_2O_6$, $CaTiAl_2O_6$, $CaFe_3AlSiO_6$ and $CaFe^{3+}{}_2SiO_6$ components, calculated according to the method of Smyth (1980) and Dunworth & Wilson (1998)]. The pyroxenes in the silica-undersaturated rocks have high Al content (up to 34% CaTs components), with some samples having >0·4 Al atoms per formula units (p.f.u.) based on six oxygens. This is typical of silica-undersaturated alkaline rocks (Le Bas, 1962) and is due to the increasing activity of Al_2O_3 as silica activity decreases (e.g. Deer *et al.*, 1978, p. 340). Molecular Al and Si contents show a very strong negative correlation and those pyroxenes with Si < 1·8 (Fig. 4) contain a significant excess of Al above that which can be accommodated in tetrahedral sites, and this excess

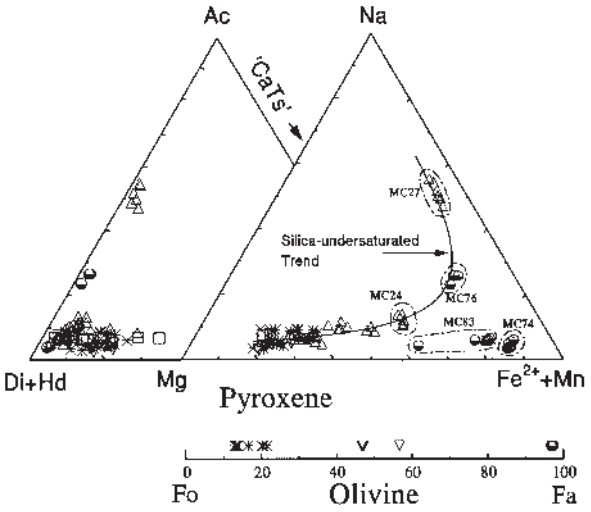

Fig. 3. Pyroxene compositions from the Messum core rocks plotted on Na–Mg–(Fe^{2+} + Mn) and acmite (Ac)–diopside + hedenbergite (Di + Hd)–Ca Tschermak (CaTs) triangles. 'CaTs' includes $CaAl_2Si_2O_6$, $CaTiAl_2O_6$, $CaFe_3AlSiO_6$ and $CaFe^{3+}{}_2SiO_6$ components, calculated according to the method of Smyth (1980) and Dunworth & Wilson (1998). The compositional range of olivines is also indicated. Symbols as in Fig. 2.

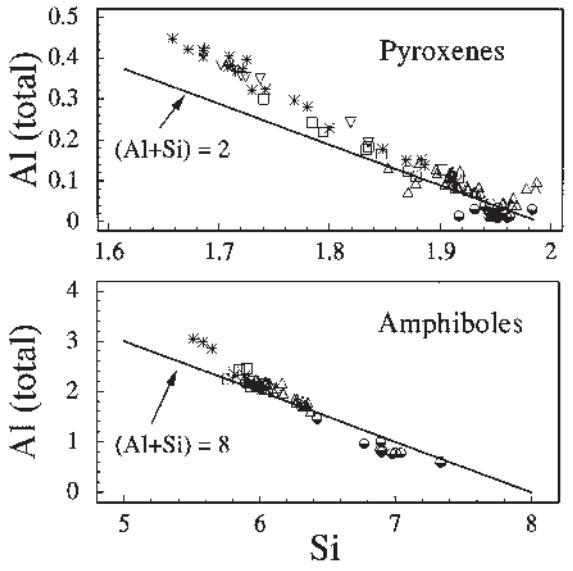

Fig. 4. Total aluminium vs Si in pyroxenes and amphiboles. Line is locus of points for which Si + Al = 2 cations (pyroxene) and Si + Al = 8 (amphibole). Pyroxenes and amphiboles above the line must have Al in six-fold sites (see text). Amphibole analyses have been normalized so that the sum of (Si + Al + Ti + Fe + Mn + Mg) = 13 cations before plotting. Symbols as in Fig. 2.

increases with increasing Al content. Five pyroxene analyses contain >9 wt % Al_2O_3, and one has 10·14 wt % Al_2O_3.

Most of the pyroxenes contain some Na (Fig. 3) and the most Na-rich pyroxene, with ~60% of the $NaFe^{3+}Si_2O_6$ molecule present, occurs in samples of nepheline syenite. The trend for the silica-undersaturated suite is typical (Deer *et al.*, 1978, p. 509). Pyroxene in quartz syenite sample MC76 lies on the silica-undersaturated trend whereas pyroxene in quartz syenite samples MC83 and MC74 approaches hedenbergite in composition (Fig. 3). Sample MC76 (SiO_2 63·60 wt %) is the least evolved of the three quartz syenites, containing only minor modal quartz, whereas samples MC83 (SiO_2 65·32 wt %) and MC74 (SiO_2 73·55 wt %) are more evolved. On the basis of the limited number of samples available, there appears to be no simple relationship between silica content of the quartz syenites and pyroxene composition.

As discussed above, both Korn & Martin (1954) and Mathias (1957) considered that that the theralites were metasomatized 'screens' of earlier tholeiitic gabbro that had become engulfed in silica-undersaturated magma and transformed to a nepheline-bearing gabbro. The pyroxenes in these rocks all have high Al_2O_3 content in both cores and rims (see Table 1), which is entirely consistent with crystallization from a silica-undersaturated magma. Hence, there is no evidence for relict tholeiitic minerals in these rocks, which are more likely to have crystallized from relatively undi erentiated versions of the magmas that produced the nepheline syenites.

Amphibole

Like the pyroxenes, the amphiboles in the silica-undersaturated rocks are notable for their high Al contents, and Fig. 4 shows that Al and Si show a strong negative correlation. Amphiboles from the nepheline syenites and dykes lie above the Si + Al = 8 line in Fig. 4, which shows that some Al occupies octahedral sites. The maximum Al_2O_3 content occurs in dyke sample MC18, where the three analysed amphiboles have between 15·9 and 17·1 wt % Al_2O_3, corresponding to 2·3 and 0·5 Al p.f.u. in four-fold and six-fold coordination, respectively. Amphiboles from the quartz syenite samples generally have (Al + Si) < 8, suggesting that some Ti might be present in tetrahedral sites.

The *mg*-number observed in amphiboles from the dykes and the nepheline syenites ranges from 0·25 to 0·7. Most contain >0·5 p.f.u (Na + K) in the A site, <0·5 p.f.u. Na in the B site, and >1·0 (Ca + Na) p.f.u. in the B site, and therefore belong to the sodic–calcic amphibole group as defined by Leake *et al.* (1997). The exact distribution of elements between sites depends on the Fe^{2+}/Fe^{3+} recalculation procedure followed (e.g. Leake *et al.*, 1997). Before plotting in Fig. 5, amphibole analyses were normalized so that the sum of (Si + Al + Ti + Fe + Mn + Mg) = 13 cations [as recommended by Leake *et al.* (1997) for the purposes of nomenclature]. Figure 5 shows that most amphiboles from the silica-undersaturated rocks have between 5·5 and 6·5 Si p.f.u. and cluster around

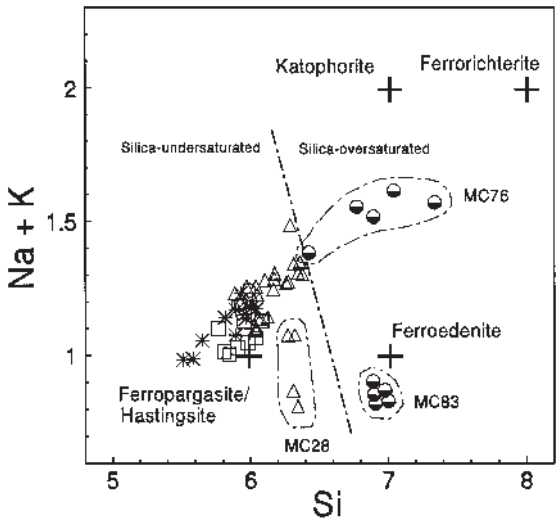

Fig. 5. Na + K vs Si for amphiboles with various end-member compositions plotted. Amphibole analyses have been normalized so that the sum of (Si + Al + Ti + Fe + Mn + Mg) = 13 cations before plotting. Symbols as in Fig. 2.

ferropargasite–hastingsite. The majority have <0·5 Al^{vi} p.f.u. and are therefore hastingsites.

Three samples (MC28, MC76 and MC83) contain amphibole that is distinct in composition from the majority of samples. Sample MC28, which is a nepheline-bearing syenite, contains hastingsite with lower alkali content than the amphiboles in the other nepheline syenites. The two quartz syenites (MC76 and MC83) are distinguished by their higher Si contents (>6·5 p.f.u.) and lower *mg*-number (~0·2). The amphiboles in MC83 show a restricted range in composition close to ferroedenite, whereas amphiboles from MC76 straddle the boundary between ferroedenite and katophorite (at Na + K = 1·5). It should be noted that the most evolved quartz syenite (MC74) does not contain amphibole. There is, therefore, the same distinction between amphibole compositions in MC76 and MC83 as seen in the pyroxenes. As in the case of the pyroxenes, there appears to be no systematic variation in amphibole compositions among the quartz syenites.

Feldspar

The theralite sample (MC3) contains plagioclase with cores of An_{66} and rims of An_{41}. The least evolved nepheline syenites, MC4 and MC44, contain plagioclase of $An_{45–30}$ and $An_{76–40}$. The nepheline syenites and syenites contain alkali feldspar with exsolution that is too coarse to be suitable for microprobe analysis. One of the fine-grained nepheline syenite dykes (MC33) contains unexsolved groundmass alkali feldspar (An_4, Ab_{60}, Or_{36}, Table 1).

Nepheline, biotite and oxide phases

The *mg*-number in biotites ranges from 0·2 to 0·6. The quartz syenites have biotite *mg*-number of 0·25, but the most iron-rich biotites are from nepheline syenite sample MC27. Little variation in nepheline composition is seen throughout the samples analysed from the silica-undersaturated suite. K_2O varies from 4·2 to 6·1 wt %. The quartz syenites contain predominantly Ti-magnetite, but primary ilmenite was found to be present in MC83. In the dykes and nepheline syenites, where opaque oxides were present they were found to be Ti-magnetite, except in the case of MC11, where ilmenite was present.

WHOLE-ROCK CHEMISTRY

Essential geochemical features are summarized in Figs 6–9 and selected analyses are reported in Table 2. The distinction between the alkaline and subalkaline suites is evident in most of the variation diagrams. The theralites exhibit limited geochemical variation, and with low SiO_2, K_2O and Na_2O, and high MgO, FeO and CaO they are compositionally the most primitive rocks in the suite in terms of *mg*-number (64–69; $n = 6$). As pointed out above, however, some basanite dykes (maximum *mg*-number = 62) carry olivine phenocrysts of higher Fo content. This character is also reflected in their high Cr, Co and Ni contents and, in keeping with the alkaline a nities of these rocks, Rb, Nb, P_2O_5, Ba and Sr are also high. With similarly low SiO_2, the phonotephrite dykes are more variable in composition, being enriched in Al_2O_3, Na_2O, K_2O, P_2O_5, Sr, Ba and Nb, and depleted in CaO, FeO, MgO, TiO_2, Zr, Co and Sc. The Cr, Ni and V concentrations in the dykes and theralites show considerable overlap.

Likewise, the nepheline syenites (including nepheline monzonites, and nepheline-bearing syenites) are also compositionally variable. With increasing SiO_2, concentrations of FeO, MgO, CaO, TiO_2, P_2O_5, Sr, Y, Co and V decrease, and those of Al_2O_3, K_2O, Na_2O, Rb and Zr increase. Data for Ba, Sr and Nb are scattered and concentrations of Ni and Cr are very low. The compositions of the least evolved members of the nepheline syenite suite approach or overlap those of the phonotephrite dykes (Figs 6–8).

The most evolved members of the nepheline syenite suite have distinctly lower Ba, Sr and CaO, and high Rb contents indicating that they are highly fractionated. Their Co, Cr, V and Cu contents are very low, and Nb, Y, Zn and Zr are highly variable, with high concentrations in those rocks with conspicuous titanite and other accessory phases. In a plot of SiO_2 vs Al_2O_3 (Fig. 6), the evolved nepheline syenites (having the highest SiO_2 contents) define a negative correlation extending from

Table 2: Selected whole-rock analyses

	Silica-undersaturated suite														Quartz syenite suite			
	Theralites			Dykes				Nepheline syenite										
	MC1	MC3	MC48	MC18	MC27	MC33	MC37	MC4	MC11	MC24	MC28	MC34	MC41	MC42	MC43	MS	MC74	MC76	MC83
SiO_2	45·10	43·54	47·24	44·08	56·44	51·98	44·32	52·26	48·96	53·41	58·31	61·60	54·79	44·18	44·11	62·83	72·68	62·01	64·51
TiO_2	1·35	1·52	1·36	1·22	0·14	1·14	1·10	1·16	1·69	0·64	0·48	0·35	0·41	1·05	1·18	0·66	0·27	0·61	0·56
Al_2O_3	15·18	15·40	16·86	16·44	21·81	20·03	18·90	21·89	19·39	21·10	20·05	19·71	20·99	20·37	19·49	16·58	12·75	16·94	16·00
FeO*	9·18	9·73	8·82	9·22	2·61	6·53	8·56	5·19	7·96	5·28	4·35	3·05	4·16	7·18	7·59	6·34	3·32	4·39	4·88
MnO	0·17	0·18	0·18	0·19	0·13	0·18	0·20	0·13	0·19	0·17	0·16	0·09	0·15	0·19	0·19	0·20	0·07	0·19	0·23
MgO	9·76	8·22	7·84	7·52	0·17	1·93	5·44	1·72	3·25	1·19	0·65	0·54	0·73	2·75	3·65	0·60	0·04	0·35	0·31
CaO	10·59	12·43	9·51	10·50	1·04	4·31	8·37	7·32	7·38	3·27	1·89	1·77	1·92	6·37	7·56	2·43	0·59	1·52	1·30
Na_2O	3·59	4·10	4·56	4·48	10·40	6·80	6·77	5·39	5·01	7·82	7·92	6·05	8·47	6·67	6·40	5·56	3·83	5·85	5·26
K_2O	1·69	2·00	2·55	2·32	5·22	4·14	2·96	2·28	2·79	5·15	5·48	6·54	6·02	4·61	4·33	4·65	5·27	5·56	5·65
P_2O_5	0·38	0·47	0·47	0·59	0·02	0·61	0·97	0·54	0·79	0·37	0·16	0·10	0·18	0·78	0·77	0·14	0·01	0·08	0·06
H_2O^-	0·07	0·08	0·09	0·38	0·13	0·28	0·17	0·08	0·12	0·12	0·04	0·19	0·24	0·76	0·45	—	0·91	0·08	0·30
LOI	1·46	1·83	1·28	3·16	2·00	1·67	3·66	1·60	1·94	1·51	0·59	0·90	2·90	3·62	3·18	0·49	0·58	1·77	0·86
Total	98·53	99·51	100·75	100·09	100·10	99·60	101·42	99·57	99·48	100·03	100·09	100·88	100·97	98·52	98·93	100·00	100·32	99·36	99·91
Nb	66	81	86	101	186	123	129	54	147	107	159	60	58	151	137	150	45	169	158
Zr	148	133	165	117	997	314	148	117	180	283	587	209	152	118	118	678	466	610	540
Y	22	24	23	21	64	29	21	21	36	23	55	15	14	18	18	90	78	60	50
Sr	688	889	662	1208	64	689	1564	1102	1224	613	119	175	238	1800	1642	152	54	24	14
Rb	49	52	68	60	369	157	70	61	72	167	220	174	197	130	118	161	193	210	206
Th	3	4	6	8	17	12	9	4	7	11	22	9	4	8	9	20	17	17	9
Pb	4	3	5	6	16	8	8	4	5	11	17	16	8	4	6	16	18	16	13
Co	51	46	42	44	3	10	31	9	18	6	n.d.	4	4	21	25	2	n.d.	n.d.	n.d.
Cr	492	265	338	338	3	4	260	8	20	8	16	6	9	7	50	6	3	4	7
V	213	229	164	185	n.d.	43	142	51	119	26	13	10	12	120	142	n.d.	n.d.	n.d.	3
Zn	67	68	64	67	64	72	69	50	68	69	71	33	49	75	69	114	82	87	83
Cu	64	111	73	68	n.d.	14	49	10	32	13	6	7	8	21	32	14	15	4	15
Ni	240	155	175	159	n.d.	n.d.	137	2	10	n.d.	6	2	4	2	21	n.d.	n.d.	n.d.	n.d.
Ba	797	941	985	1182	99	1217	994	2093	1612	1226	419	820	495	2025	1828	1312	1020	257	110
Sc	24	25	18	15	n.d.	3	8	6	74	2	2	1	b.d.	2	6	7	0	0	0

MC1, theralite, base hill I; MC3, theralite, base hill III; MC48, theralite dyke, hill 1; MC18, dyke; MC27, Ne syenite dyke, W plug IV; MC33, Ne syenite dyke, S hill IV; MC37, basanite dyke, W hill IV; MC4, ne syenite (f), base plug III; MC11, ne syenite (h), hill II; MC24, ne syenite (f), NE of plug III; MC28, ne syenite (f), W of hill IV; MC34, ne syenite (f), hill IV; MC41, ne syenite (h), summit hill I; MC42, ne syenite (h) hill I; MC43, ne syenite (h), hill I; MS, average quartz microsyenite (n = 13); MC74, qz syenite, Cave Hill; MC76, quartz syenite; MC83, qz syenite, W end Camp Hill. n.d., not detected; b.d., below detection limit. For nepheline syenites, h indicates collected from central hills and f indicates collected from flat areas (see text).

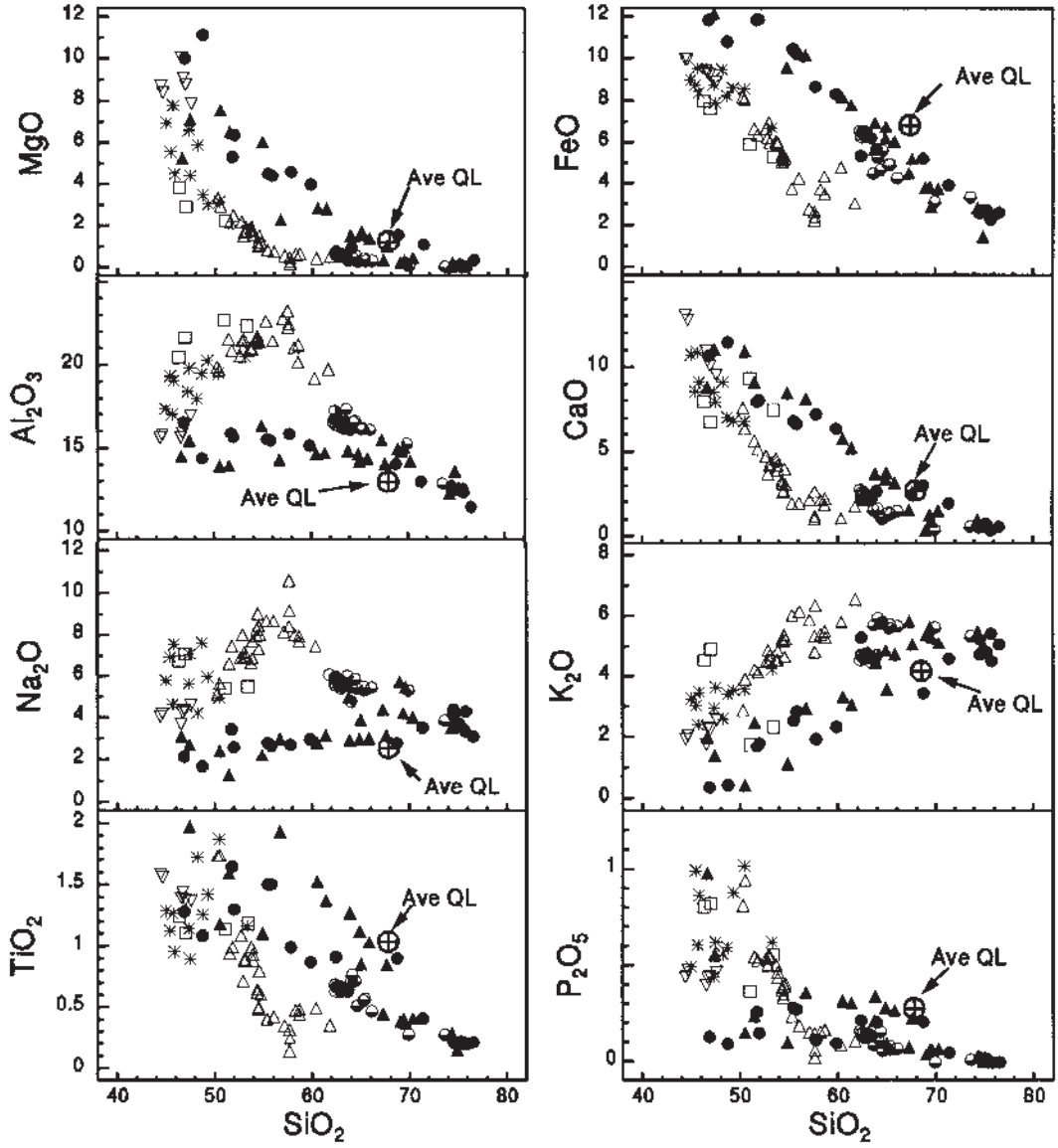

Fig. 6. Selected oxides vs silica; symbols as for Fig. 2. The average composition of the quartz latite units erupted from Messum (Ewart *et al.*, 1998*b*) is indicated.

close to the composition of the 0·1 GPa phonolite minimum in the system SiO_2–$NaAlSiO_4$–$KAlSiO_4$–H_2O towards the evolved silica-oversaturated compositions. This suggests that not all of these evolved nepheline syenites lie on the same closed-system liquid line of descent from the less evolved nepheline syenites.

Those members of the primitive nepheline syenite suite (MC4, MC44, MC42 and MC43) with unusual compositions are clearly evident in SiO_2 vs K_2O and in CaO vs Al_2O_3 as well as several other plots. MC4 and MC44 are petrographically similar to other primitive nepheline syenites (nepheline monzonites) but are characterized by lower K, Nb, Na and Rb, and higher Ca, Al and Sr. This is suggestive of plagioclase accumulation, or the plagioclase is more calcic, or both. MC42 and MC43 show compositional a nities to the phonotephrite dykes and show petrographic a nities to these rocks as well. Compared with the dykes these two samples are richer in K, Al, Ba and Rb, and poorer in Mg.

The quartz syenites, quartz microsyenites and granitic di erentiates are all more SiO_2 rich than the undersaturated rocks. The quartz syenites and quartz microsyenites cluster in two groups on the TAS diagram (Fig. 2) and many other variation diagrams (Figs 6–8). Thus in the quartz syenite–microsyenite suite, there is a bimodal distribution of compositions. The quartz micro-

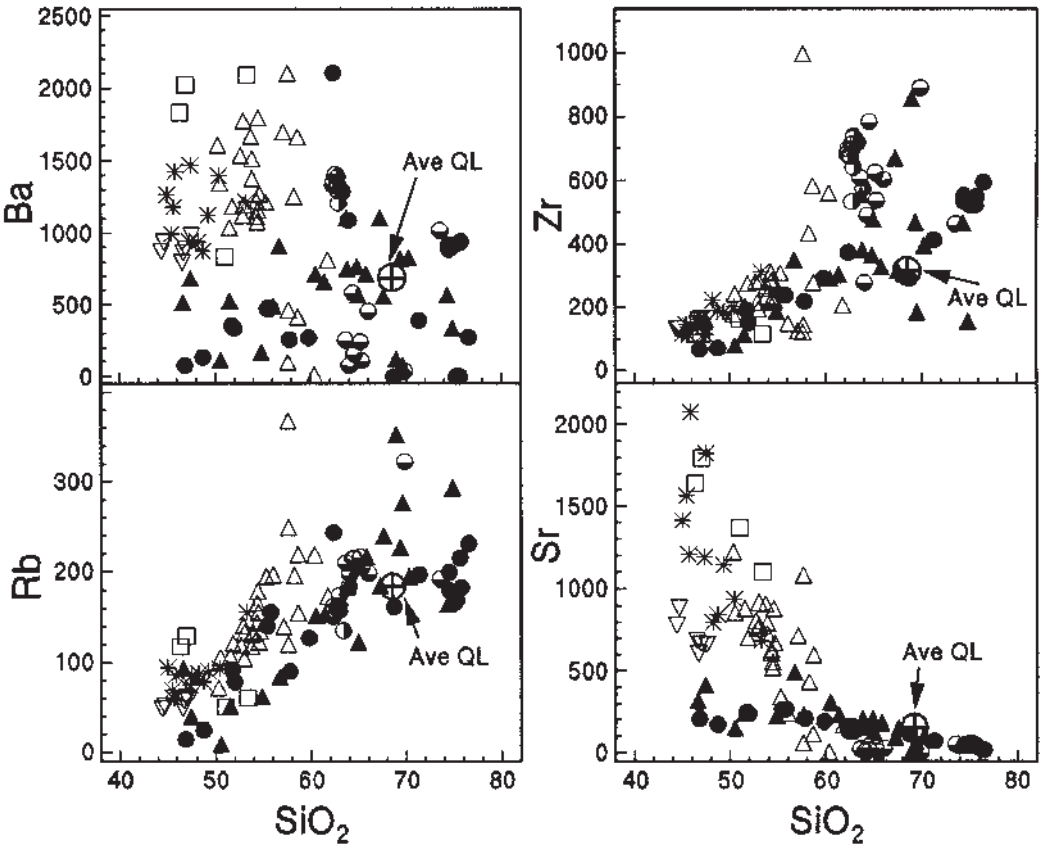

Fig. 7. Selected trace elements vs silica; symbols as for Fig. 2. The average composition of quartz latite erupted from Messum is also indicated (Ewart *et al.*, 1998*b*).

syenites have lower K_2O and Rb, and higher MgO, FeO, CaO, Sr and Ba than the quartz syenites, but there is no di erence in Zr, Y and Nb contents, which are fairly scattered for both groups of samples. Taken as a whole, the quartz syenite–microsyenite suite shows a general decrease in Ti, Al, Fe, Ca, Mg, P, Na, Nb and Zn, and a general increase in Rb with increasing SiO_2. The quartz syenite–granite group of rocks are highly fractionated in terms of low Sr and high Zr and Nb.

The subalkaline suite of breccias and hornfelsed volcanic rocks has much higher MgO, FeO, CaO and TiO_2, and lower Al_2O_3, Na_2O and K_2O content than the silica-undersaturated suite for a given SiO_2 content (Figs 2 and 7), and generally lower Sr, Ba and Rb content (Figs 7 and 8). Quartz latites erupted from Messum (Goboboseb QL units I and II; Ewart *et al.*, 1998*b*) have average SiO_2 contents of 67·93 wt % (unit I) and 67·64 wt % (unit II). Their average compositions lie within the spread of data points for the sub-alkaline suite on all the variation diagrams shown in Fig. 2 and Figs 6–8. Therefore, at least some of the sub-alkaline suite could represent blocks of quartz latite that subsided into the core of the complex during the subsequent development of the volcano.

Chondrite-normalized REE profiles for a variety of rock types are shown in Fig. 9. Clearly, the profiles are influenced by the fact that most of the rocks are cumulates and do not represent liquids. The basanite dyke (MC37) shows strong enrichment of the light rare earths with a flattening of the profile over the heavy rare earths. The theralite (MC3) shows a very similar profile, with slight depletion of La–Eu and slight enrichment of Gd–Lu compared with MC37. Most of the nepheline syenites have a lower REE content than MC3 and MC37 with a more pronounced concave-up curvature of the profile. Two samples show no Eu anomaly, one sample shows a positive Eu anomaly, and MC28, with the highest REE content, shows a strong negative Eu anomaly with a pronounced flattening of the profile from Gd to Lu. The quartz syenite suite have REE profiles similar to that of MC28. The quartz syenite (MC74) with the highest SiO_2 content (72·68 wt %) has the highest REE content and an REE profile that is very similar to the quartz microsyenite sample (MC53). Figure 9(d) gives the REE profiles for Tristan da Cunha basanite and various Etendeka magma types for comparison and these are discussed in a later section.

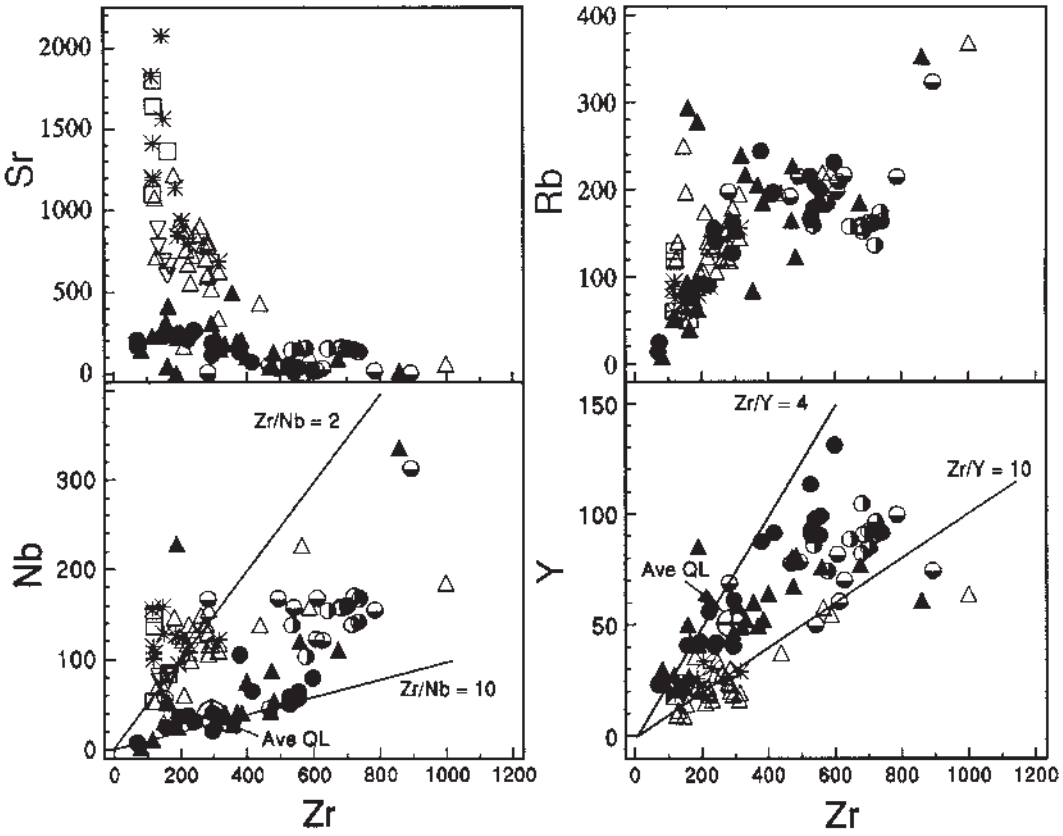

Fig. 8. Selected trace elements vs Zr; symbols as for Fig. 2. The average composition of quartz latite erupted from Messum is also indicated (Ewart *et al.*, 1998*b*).

ISOTOPE DATA

Harris (1995) has discussed the oxygen isotope geochemistry of the Mesozoic anorogenic complexes of Namibia, and data for the Messum Core samples (plus an additional analysis) are given in Table 3. The $\delta^{18}O$ values of the original magmas (δ_{magma}) have been estimated from the $\delta^{18}O$ values of one or more of the constituent minerals (see Harris, 1995). Strontium isotope data for nine samples and Nd-isotope data for five samples are also reported in Table 3. Estimates of the $\delta^{18}O$ values of the magmas range from 6·0 to 8·0‰, the silica-undersaturated samples having lower $\delta^{18}O$ values (6·0–6·9‰) than the silica-oversaturated samples (7·2–8·0‰). Three samples from the quartz syenite suite have $\delta^{18}O$ values ranging from 7·2 to 7·8‰.

The initial Sr-isotope ratios in the silica-undersaturated suite (Table 3) show a restricted range from 0·70447 to 0·70487, whereas three samples of quartz syenite show higher and more varied values (0·70552–0·70789). However, because of the high Rb/Sr ratios in the quartz syenites (3·6–14·2), the calculated initial ratio is highly sensitive to the age chosen for the rock. Sample MC74, however, has a relatively low Rb/Sr ratio (3·6) and within the spread of possible ages allowed by the published dates and their errors (125·5–130·0 Ma) has an initial Sr-isotope ratio ranging from 0·7076 to 0·7083, which is significantly above those of the silica-undersaturated suite. The initial Nd-isotope ratios of the four silica-undersaturated rocks analysed range from 0·51260 to 0·51264 with slight positive ε_{Nd} values. The single quartz syenite sample analysed (MC74) has a lower initial Nd-isotope ratio of 0·51251 and slight negative ε_{Nd} value.

PETROGENESIS

Mafic rocks and parental magmas

A major obstacle in identifying petrogenetic lineages among the alkaline core rocks is that most rocks probably do not represent liquid compositions. The most obvious candidates for parental magmas within the core rocks are the theralites, which have low silica (44–46 wt %) and relatively high MgO content (8–10 wt %; *mg*-number 64–69). Although they seem to have been intruded after the nepheline syenites, it is possible that they crystallized from liquids equivalent in composition to those from

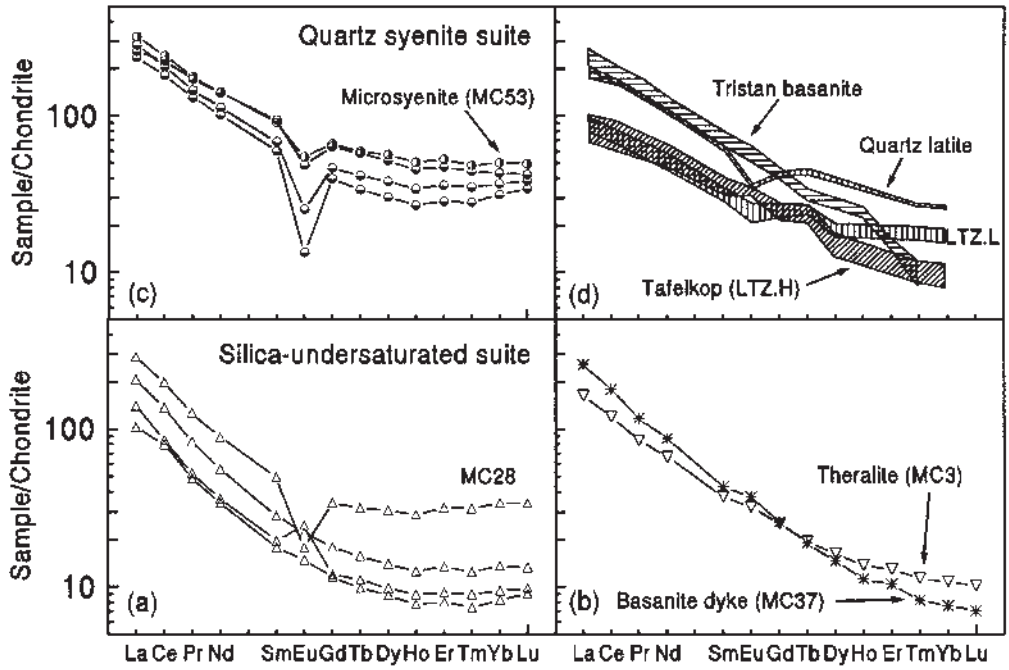

Fig. 9. Chondrite-normalized REE plots for selected Messum core samples. The range for Tristan basanites (A. P. le Roex, personal communication, 1999), quartz latite erupted from Messum (Goboboseb and Springbok Units, Ewart *et al.*, 1998*b*) and Tafelkop (LTZ.H, low Ti–Zr, high Ti/Zr) and LTZ.L (low Ti–Zr, low Ti/Zr) basalts (Ewart *et al.*, 1998*a*) are shown for comparison in (d).

which the nepheline syenites evolved. Figure 10 shows the major plutonic silica-undersaturated rock types (theralites and nepheline syenites) plotted on various oxide vs SiO_2 diagrams with the compositional range of the phenocrysts in these groups of rocks also shown. The data array can be qualitatively explained by crystal fractionation of olivine, plagioclase and clinopyroxene from a theralite-like composition in the appropriate proportions. There appear to be two compositionally distinct groups within the theralites, with one group having higher CaO and lower SiO_2 than the other. These di erences cannot simply be explained in terms of di erences in crystal content because Al_2O_3 is the same in both groups (therefore not plagioclase control) and the high CaO group do not have high Cr content (Fig. 11).

The compositional trends show several important features (Fig. 10). There is a change in gradient of the CaO vs MgO trend between the theralites and the nepheline syenites, which suggests a greater importance for pyroxene fractionation once MgO contents dropped below ~5 wt %. The increasing dominance of feldspar (and possible nepheline) fractionation as SiO_2 increases above ~58 wt % can be seen on the Al_2O_3 vs SiO_2 plot but feldspar fractionation must also be involved in formation of the theralites. On the CaO vs SiO_2 plot, the trend becomes almost horizontal and lies along a line joining alkali feldspar and nepheline. Re-emphasizing that these compositions are unlikely to correspond to liquids, the compositional variation in the evolved rocks can best be explained by variations in the proportions of nepheline and alkali feldspar.

Further constraints on the likely fractionating minerals are given by Fig. 11, where Al_2O_3, FeO, Cr and Sr are plotted against MgO. In this case, all the mafic dyke data are plotted as well. The FeO vs MgO curve is similar to that of CaO vs MgO (Fig. 10) in that it steepens with declining MgO content. Cr, on the other hand, shows a continual decline as MgO decreases down to MgO ~ 3 wt %, when the Cr content becomes zero. These two observations are consistent with continuous fractionation of pyroxene, and the onset of magnetite fractionation from MgO < 3 wt %. The plots of Al_2O_3 and Sr vs MgO are similar. The Al_2O_3 content increases with decreasing MgO from 10 to ~2 wt %, and shows a sudden decline for MgO less than ~2 wt %. Sr shows a general increase with MgO up to about MgO = 5 wt % then shows a steep decline as MgO decreases further. These plots are consistent with feldspar fractionation below MgO ~ 5 wt %. This is consistent with the lack of Eu anomaly in the dyke (MC37) and theralite (MC3), which contain 5·44 and 8·32 wt % MgO, respectively.

Variations within the nepheline syenites

The central core of nepheline syenites contains rocks which range from nepheline syenites with >10 modal %

Table 3: Oxygen, strontium and neodymium isotope data

Sample	Rock type	SiO_2n	δ qtz	δ fsp	δ p/a	δ bi	δ_{magma}	$^{87}Sr/^{86}Sr$	$(^{87}Sr/^{86}Sr)_i$	ε_{Sr}	$^{143}Nd/^{144}Nd$	$(^{143}Nd/^{144}Nd)_i$	ε_{Nd}
Silica-undersaturated suite													
MC3	Theralite	44·61		7·2	6·0		6·8	0·704793(14)	0·70449	0·09	0·51263(2)	0·51254	2·07
MC4	Ne syenite	53·38		7·2	5·7[a]	5·8	6·5	0·704930(20)	0·70464	2·33			
MC11	Ne syenite	50·26		6·5			6·8						
MC18	Dyke	45·66			6·0		6·0						
MC24	Ne syenite	54·28		7·4	5·2[a]		6·0	0·706071(11)	0·70464	2·26			
MC28	Ne syenite	58·63		8·2	5·9[a]		6·7	0·714596(14)	0·70487	5·48	0·51266(3)	0·51256	2·57
MC34	Ne syenite	61·73			5·8[a]		6·6	0·710086(14)	0·70486	5·33	0·51260(4)	0·51252	1·62
MC37	Dyke	45·41			6·1		6·9	0·704703(13)	0·70447	−0·16	0·51264(1)	0·51256	2·45
MC41	Ne syenite	56·01			5·8		6·6						
MC44	Ne syenite	51·00		7·5	5·7[a]		6·5						
Quartz syenite suite													
MC74	Granite	73·55	9·8				7·8	0·726720(26)	0·70789	48·3	0·51251(3)	0·51240	−0·57
MC76	Qz syenite	69·87	9·2				7·2	0·750089(34)	0·70581	18·9			
MC83	Qz syenite	65·32	9·4				7·4	0·781129(16)	0·70552	14·7			
Sub-alkaline suite													
MC80	Dyke	69·35	9·0				8·0						
MC60	Dyke	76·50	8·2				7·2						

All stable isotope data except MC75 from Harris (1995). p/a, pyroxene and/or [a]amphibole. $\delta_{magma} = \delta^{18}O$ value of magma and assumes $\Delta_{quartz\text{-}magma} = 1{\cdot}0‰$ (dykes) and 2·0‰ (quartz syenite), $\Delta_{pyroxene/amphibole\text{-}magma} = -0{\cdot}8‰$ and $\Delta_{feldspar\text{-}magma} = +0{\cdot}3‰$. Figures in parentheses after $^{87}Sr/^{86}Sr$ value are 1 SE on measured ratios and refer to least significant digit(s). SiO_2n is SiO_2 normalized to 100% volatile free. Rb and Sr data for age correction given in Table 4. Samples MC76 and MC83 have <30 ppm Sr. Sr in these samples was determined by XRF with extended counting times and ICP-MS. MC76 gave 24·51 ± 0·58 (XRF) and 25·0 ± 0·96 (ICP-MS); MC83 gave 14·11 ± 0·56 (XRF) and 14·5 ± 0·32 (ICP-MS) where uncertainty is 2σ based on counting statistics.

nepheline to syenites with little or no nepheline. Figure 12 shows that the nepheline syenites from the four intrusions have consistently lower CaO, higher total alkalis and lower SiO_2 than those rocks from the flat areas. The nepheline syenites from the hills form a coherent suite that trends towards the phonolite minimum at 0·1 GPa and is, therefore, consistent with closed system crystal fractionation. The nepheline syenites from the flat areas form an array (Fig. 12) that curves towards the composition of the quartz syenites as SiO_2 increases. This suite cannot represent a closed system liquid line of descent.

Rocks from both suites ('hills' and 'flats') have very similar compositions at silica contents of around 52–55 wt %, then diverge at higher silica contents. Three possible explanations for the presence of two distinct silica-undersaturated suites are as follows. First, the nepheline syenites of the flat areas could have formed from quartz syenite that became fenitized before or during intrusion of the nepheline syenites that form the four hills. This process would require an influx not only of alkalis, but also of Ca (which is unlikely). Although in accordance with the earlier interpretations of Korn & Martin (1954) and Mathias (1956), there is no petrographic evidence to support such a model. A second explanation is that the nepheline syenites in the flat areas could have assimilated some of the surrounding quartz syenite during di erentiation and emplacement. They would then have acted as a bu er between the quartz syenites and the later intrusions of nepheline syenite magma, preventing them from becoming contaminated. The third explanation is that the nepheline syenites from the flat areas are enriched in cumulus alkali feldspar, which drives them towards syenite in composition (Fig. 12).

The REE profiles (Fig. 9) indicate that both alkali feldspar accumulation and contamination by quartz syenite occurred. Although nepheline syenite sample MC34 plots closest to the quartz syenite field in Fig. 12, it has a similar REE profile to MC24 and MC41, which plot within the field that trends to the phonolite minimum. However, MC34 has a positive Eu anomaly, which indicates that significant feldspar accumulation occurred. Nepheline syenite MC28, which is one of the group of

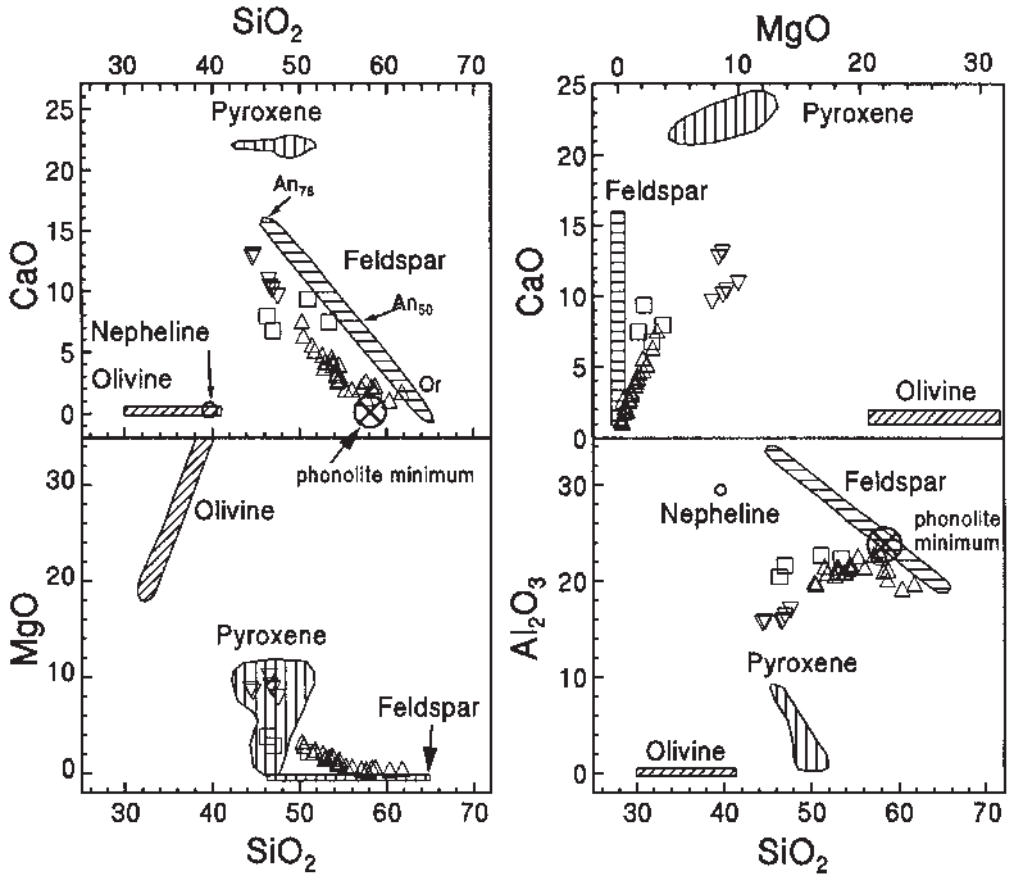

Fig. 10. Selected oxides vs silicates for silica-undersaturated plutonic samples only; symbols as for Fig. 2. Fields for mineral compositions from these rock types also plotted. The approximate position of the 0·1 GPa phonolite minimum in the system quartz–nepheline–kalsilite–water (Schairer, 1950) is indicated.

samples that plot towards quartz syenite in Fig. 12, has an REE profile that has a strong negative Eu anomaly, indicating that this sample is not enriched in cumulus feldspar. Furthermore, the similarity in REE profile with the quartz syenites is consistent with contamination of the nepheline syenite parent magma by quartz syenite. Cumulus enrichment of alkali feldspar is unlikely to be the main cause of the trend towards quartz syenite in Fig. 12. Sample MC34 is noticeably more coarse grained than the other nepheline syenites from the flat areas, which show no petrographic evidence for cumulus enrichment. We therefore favour a mechanism involving contamination by quartz syenite. Further evidence for, and the nature of, the crustal contamination processes a ecting the Messum core rocks are discussed below.

The four samples that have so far been treated as an anomalous group (MC4, MC42, MC43, MC44) may not be closely related petrogenetically to the two undersaturated suites in that they could represent partially metasomatized xenoliths of earlier material (but there is no field evidence to confirm this hypothesis). It is interesting to note (Fig. 12) that the two samples from within one of the 'hills' (MC42 and MC43) are considerably richer in alkalis and poorer in silica than the two samples collected from the flat areas (MC4 and MC44), thus the relationship is in the same sense as for the host material.

Silica-oversaturated suite

It is necessary to explain, first, the variation within the quartz syenite group (including the two granite samples with $SiO_2 > 68\%$, Fig. 2) and, second, the relationship between the quartz microsyenites and the quartz syenites. The quartz syenites and granites lie on linear trends on most variation diagrams and their relationship can most easily be explained by varying proportions of alkali feldspar, quartz and ferromagnesian minerals. The quartz microsyenites are less evolved (in terms of lower SiO_2 and higher CaO), show comparatively less variation and are o set from the quartz syenite–granite trend in most variation diagrams. As discussed above, intrusion of the quartz microsyenites post-dates intrusion of the quartz

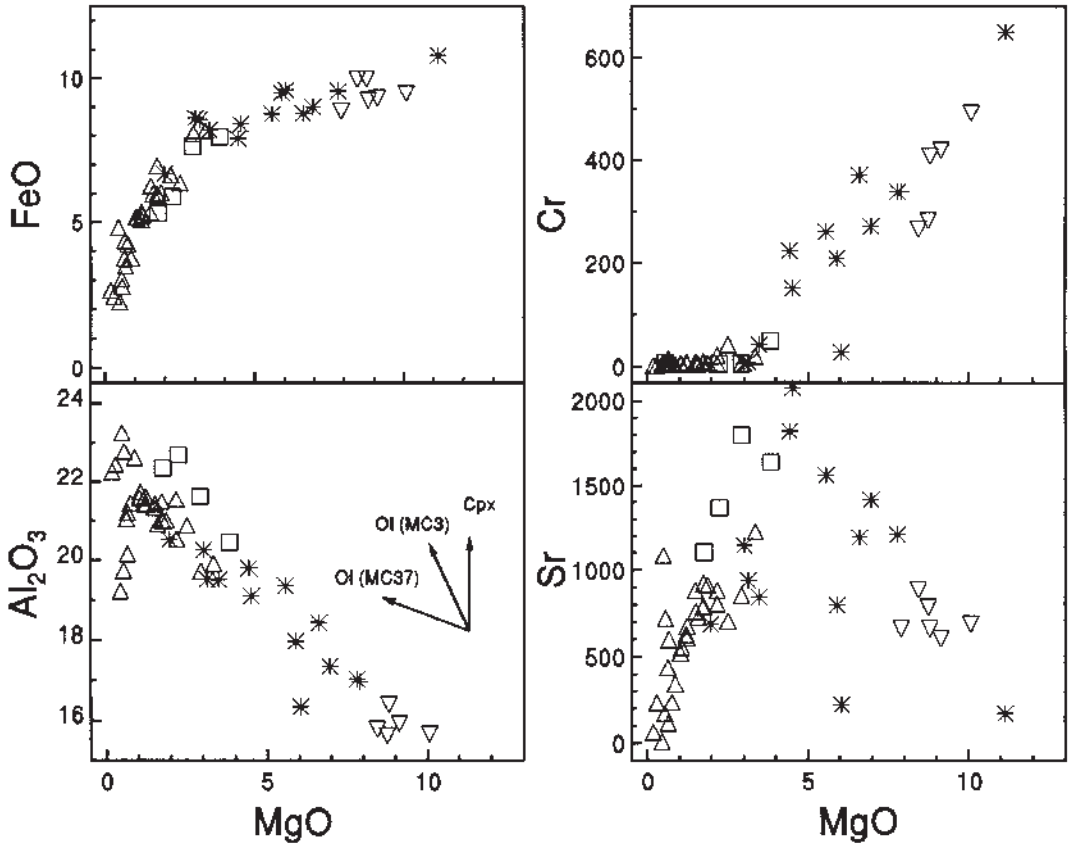

Fig. 11. Selected oxides and trace elements vs MgO; symbols as for Fig. 2. Arrows in lower left figure are crystal fractionation vectors for most MgO-rich sample (at MgO ~ 10 wt %, Al_2O_3 ~ 16 wt %).

syenite pluton. The quartz microsyenite could represent a slightly less evolved magma produced from the same source as the quartz syenites. Least-squares mixing calculations indicate that 57% removal of a mixture of alkali feldspar, plagioclase (An_{15}, core of a feldspar in quartz syenite MC74), ferroaugite, olivine and Ti-magnetite in the proportions 47:37:9:4:4 from average quartz microsyenite will closely approximate the average quartz syenite major element composition (sum of squares of residuals is 0·3). For this amount of fractionation to account for the observed di erence in Sr content (average for quartz microsyenite 150 ppm, and average for quartz syenite 25 ppm), a bulk distribution coe cient (D) for Sr of about three is implied. This is consistent with a fractionation assemblage dominated by sodic plagioclase (D ~ 2) and alkali feldspar (D ~ 5). These feldspar distribution coe cients are within published estimates (e.g. le Roex, 1985). The average quartz syenite has a slightly higher Nb content (172 ppm) than the quartz microsyenite (150 ppm) but both Zr and Y are lower in the quartz syenite (603 and 73 ppm) compared with the quartz microsyenite (678 and 90 ppm), which suggests incorporation of these elements in fractionating ferromagnesian minerals or accessory phases such as zircon. The REE profiles of Fig. 9(c) are consistent with the fractionation model described above in that the Eu anomaly in the microsyenite is smaller than in the quartz syenite samples. The lower REE content in the quartz syenites presumably reflects a combination of accessory mineral fractionation and crystal accumulation. It is therefore concluded that the quartz microsyenite magmas have a similar origin to the quartz syenites involving slightly less crystal fractionation.

Crustal contamination in the quartz syenites and nepheline syenites

Oxygen isotope data are presented in Fig. 13. Mineral $\delta^{18}O$ values have been used to estimate the $\delta^{18}O$ value of the magmas (δ_{magma}) from which they crystallized (Harris, 1995). The main feature of the data is that the silica-undersaturated rocks have values of $\delta_{magma} < 7{\cdot}0‰$, whereas the silica-oversaturated rocks (quartz syenites from the core, rocks from the sub-alkaline suite, and the outer gabbros) have values of $\delta_{magma} > 7{\cdot}0‰$. Closed

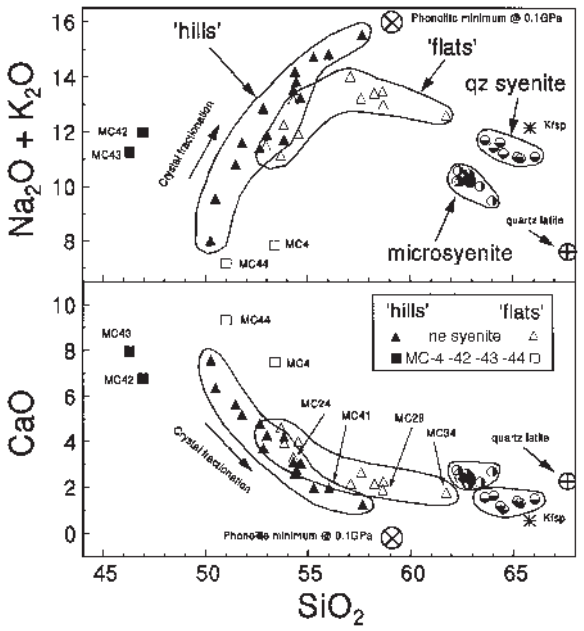

Fig. 12. Total alkalis and CaO vs silica for nepheline syenite and quartz syenite samples. Samples of nepheline syenite from the four hills ('hills') in Fig. 1 are distinguished from those collected from the low-lying areas ('flats') between the hills and the quartz syenite but within inner nepheline syenite core (Fig. 1). Also shown is the approximate position of the 0·1 GPa phonolite minimum in the system quartz–nepheline–kalsilite (Schairer, 1950), the composition of average alkali feldspar (kfsp), and the average composition of quartz latite units I and II, which were erupted from Messum (Ewart *et al.*, 1998*b*).

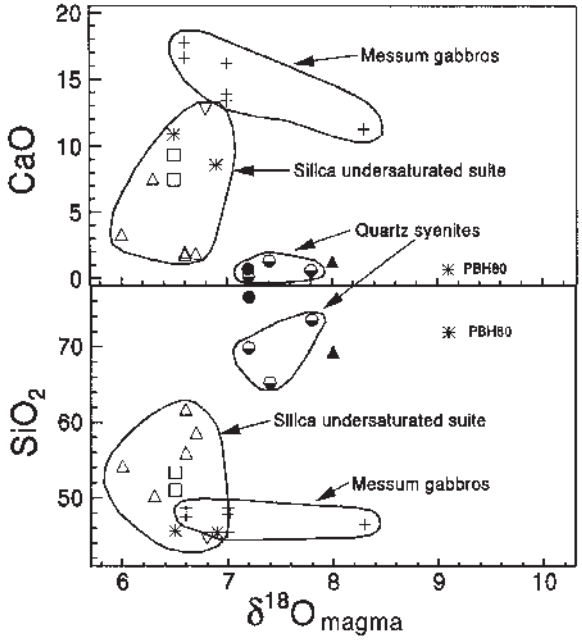

Fig. 13. CaO and SiO_2 vs $\delta^{18}O$ value of magma (δ_{magma}) calculated using mineral data and appropriate fractionation factors (Harris, 1995). Symbols as for in Fig. 2, except that the crosses (+) represent the Messum gabbros from outside the central core complex, and PBH80, a granitic sheet (SiO_2 71·89 wt %) cutting the outer gabbros, is also plotted [data from Harris (1995)].

system crystal fractionation cannot change the $\delta^{18}O$ value of a magma significantly (e.g. Sheppard & Harris, 1985) and the elevated values of δ_{magma} in the silica-oversaturated rocks suggest that crustal contamination played an important role in their petrogenesis.

The initial Sr-isotope ratio, calculated for 128 Ma, the average of the Rb–Sr and ^{40}Ar–^{39}Ar, is plotted against δ_{magma} in Fig. 14. The possible errors caused by the uncertainty in age and in Rb/Sr ratio are shown for each sample where significant (in practice, this a ects only samples MC28, MC74, MC76 and MC83). The two mafic rocks (MC3 and MC37) show relatively elevated δ_{magma} (6·8 and 6·9‰) but low initial Sr-isotope ratios, which might reflect limited crustal contamination, with the Sr-isotope ratios being bu ered by the high Sr content (>800 ppm, Table 2) of the magma. The nepheline syenites show initial $^{87}Sr/^{86}Sr$ ratios <0·705 whereas the quartz syenites have higher values up to 0·7078. As discussed above, the high Rb/Sr ratios of the quartz syenites mean that the initial $^{87}Sr/^{86}Sr$ ratio is subject to considerable error. Nevertheless, sample MC74 must have formed from a magma with much higher $^{87}Sr/^{86}Sr$ ratio than the nepheline syenites, which is consistent with the quartz syenites forming from crustally contaminated magmas. It should be noted from Fig. 9(d) that the REE profiles for the microsyenite (MC53) and quartz syenite MC74 are very similar to those of the Goboboseb and Springbok quartz latites (Ewart *et al.*, 1998).

Simple mixing and combined assimilation–crystal fractionation paths (AFC, DePaolo, 1981) are also shown in Fig. 14. The three contaminants chosen for the model are those of Martinez *et al.* (1996) and are representative of the exposed country rock (Damara granite with $\delta^{18}O$ = 11·9‰, Sr = 200 ppm, $^{87}Sr/^{86}Sr$ at 128 Ma = 0·73846; Kuiseb schist with $\delta^{18}O$ = 14·2‰, Sr = 129 ppm, $^{87}Sr/^{86}Sr$ at 128 Ma = 0·72711; southern Etendeka quartz latite with $\delta^{18}O$ = 11·6‰, Sr = 167 ppm, $^{87}Sr/^{86}Sr$ at 128 Ma = 0·72136). The starting composition was assumed to be a mantle-derived magma corresponding closely to nepheline syenite MC24 ($\delta^{18}O$ = 5·7‰, Sr = 1000 ppm, initial $^{87}Sr/^{86}Sr$ = 0·7045). The Sr-isotope ratio of this hypothetical end-member corresponds closely to that of the Tristan plume at that time (le Roex & Lanyon, 1998). In the simple mixing models, the high Sr-isotope ratios of quartz syenite MC74 could be produced by about 35% contamination with Damara granite. The other two potential contaminants do not have high enough Sr-isotope ratios at 128 Ma to have the desired e ect because of the high Sr content of the starting composition. The AFC paths shown in Fig. 14 were constructed using the equations of Taylor & Sheppard

Table 4: Rare earth element data for Messum core samples

Sample		La	Ce	Pr	Nd	Sm	Eu	Gd	Tb	Dy	Ho	Er	Tm	Yb	Lu
Silica-undersaturated suite															
MC3	Theralite	38·7	73·4	8·06	31·2	5·75	1·87	5·20	0·73	4·17	0·78	2·16	0·29	1·84	0·26
MC24	Ne syenite f	49·3	83·6	7·92	26·2	4·35	1·29	3·69	0·59	3·55	0·72	2·23	0·32	2·32	0·34
MC28	Ne syenite f	68·4	121	12·1	41·6	7·61	1·03	7·07	1·20	7·79	1·64	5·3	0·81	5·84	0·84
MC34	Ne syenite f	33·5	52·4	5·00	17·1	3·03	1·43	2·49	0·42	2·49	0·51	1·53	0·23	1·61	0·25
MC41	Ne syenite h	24·4	48·9	4·63	16·1	2·73	0·87	2·38	0·37	2·26	0·44	1·33	0·19	1·40	0·23
MC37	Dyke	60·9	109	11·2	40·4	6·62	2·17	5·34	0·71	3·74	0·64	1·72	0·21	1·30	0·18
Quartz syenite suite															
MC53	Microsyenite	76·6	150	17·0	66·9	13·9	3·18	13·7	2·22	14·4	2·88	8·82	1·24	8·55	1·26
MC74	Qz syenite	61·7	139	16·5	65·9	14·4	2·83	13·1	2·16	13·2	2·59	7·88	1·13	7·36	1·08
MC76	Qz syenite	68	128	14·0	53	10·5	1·47	9·60	1·56	9·7	1·94	5·99	0·9	6·30	0·98
MC83	Qz syenite	56·6	112	12·5	47·7	9·14	0·78	8·17	1·27	7·77	1·53	4·72	0·72	5·35	0·88

Analyses by ICP-MS. Errors are typically <2% relative. For nepheline syenites h signifies sample is from hill and f signifies that sample was collected from flat areas (see text and Fig. 1).

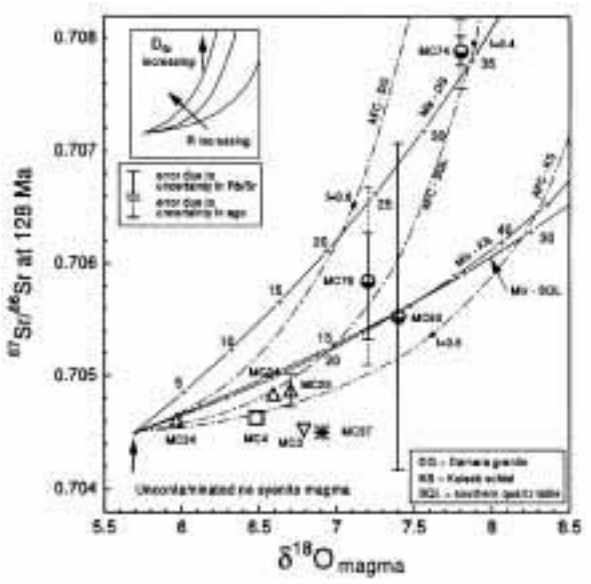

Fig. 14. Initial Sr-isotope ratio (at 128 Ma) vs $\delta^{18}O$ value of magma for Messum core samples (symbols as for Fig. 2). Error bars on samples MC28, MC76, MC83 and MC74 correspond to potential errors caused by uncertainty in age and in Rb/Sr (1σ). Simple mixing curves between a mantle-derived parent magma and Damara granite, Kuiseb Schist and Etendeka quartz latite (see text) are shown. The AFC curves assume the same starting composition and contaminants. The ratio of mass of cumulates to mass of contaminant (R) was set at three and the bulk distribution coefficient for Sr between melt and crystals, D_{Sr}, was assumed to be six. The inset diagram shows the effect of increasing D_{Sr} and R on the AFC curves.

(1986). They suffer from a lack of constraint caused by the uncertainty of the value for the bulk partition coefficient for Sr (D_{Sr}) in felsic magmas, for which the published estimates range from five to ten (e.g. le Roex *et al.*, 1990). AFC is capable of producing a much greater increase in $^{87}Sr/^{86}Sr$ than simple mixing because of the greatly reduced Sr content as fractionation proceeds. The AFC curves in Fig. 14 were calculated assuming a ratio of mass of cumulates removed to mass of material assimilated (R) of three and a value of D_{Sr} of six. It should be noted that contamination by Etendeka quartz latite is now a viable means of generating the composition of MC74 with a value of f (fraction of liquid remaining) of about 0·4. The diagram inset of Fig. 14 illustrates the effect of changing R and D_{Sr}. Higher values of the former make the curves steeper over the range of values plotted. The same value of f for the same contaminant would lie at a higher value of $^{87}Sr/^{86}Sr$ and a lower $\delta^{18}O$ value. Higher values of the latter increase only the $^{87}Sr/^{86}Sr$ for a particular f value.

It should be clear from the above that it is not possible to identify the nature of the contaminant with certainty. It is also not possible to produce well-constrained models of the contamination process that affected the early nepheline syenites preserved in the flat areas of the core because of the lack of sufficient isotope data. The curved nature of the data array (Fig. 12) is consistent with an AFC process (DePaolo, 1981) because the most evolved samples are the most contaminated.

MANTLE SOURCE CONSTRAINTS

Most of the rocks discussed in this paper are too evolved to provide reliable information about their potential

mantle source(s). It has been argued above that the silica-undersaturated suite crystallized from uncontaminated mantle-derived magmas that evolved by closed-system crystal fractionation. The initial $^{87}Sr/^{86}Sr$ ratios of the silica-undersaturated suite are slightly lower than those of the Tristan plume at 128 Ma, but lie within the range for the Tafelkop mafic magma type of the Goboboseb [Milner & le Roex (1996); termed LTZ.H, or low Ti–Zr with high Ti/Zr ratio by Ewart *et al* (1998*a*)]. Our limited Sr- and Nd-isotope data on the silica-undersaturated suite have the same characteristics as the Tafelkop basalts (Milner & le Roex, 1996) and plot within the field for the Tristan plume (see Fig. 16, below). In this regard, it should be noted that alkali gabbros, which have been interpreted as plume-derived melts (Milner & le Roex, 1996), also occur in the Okenyenya complex 100 km NE of Messum.

The dykes that cut the alkaline core of Messum represent the youngest phase of igneous activity, but their composition closely matches the least evolved rocks of the nepheline syenite suite in both major and trace element characteristics. Five samples of these basanite dykes have MgO contents >5 wt % and these are compared with the most mafic Tafelkop (LTZ.H) and LTZ.L (low Ti/Zr) lavas of Ewart *et al.* (1998*a*) in Fig. 15. There is little resemblance in trace element patterns between the Messum basanites and either of these rock types that are from the collar of earlier volcanic rocks surrounding the complex. Basanites from Tristan da Cunha with MgO > 5 wt % show normalized trace element patterns that are very similar to those of the Messum basanites. The Messum basanites show a greater enrichment of the more incompatible elements (Rb–Nb) whereas the Tristan basanites show a greater enrichment of less compatible elements (Zr–Y). The basanite and theralite samples (Fig. 9b) have very similar REE profiles to the Tristan da Cunha basanites with the exception of a slight flattening of the profile from Dy to Lu.

Ewart *et al.* (1998*a*) concluded that the Tafelkop-type (LTZ.H) lavas were dominated by mantle–plume geochemical signatures in that they have isotope and trace element characteristics intermediate between E-MORB and OIB compositions. The Messum basanite dykes, the final stage of igneous activity at Messum, show a much closer a nity to Tristan lavas than to the Tafelkop (LTZ.H) basalts and may therefore reflect a greater input from the Tristan plume.

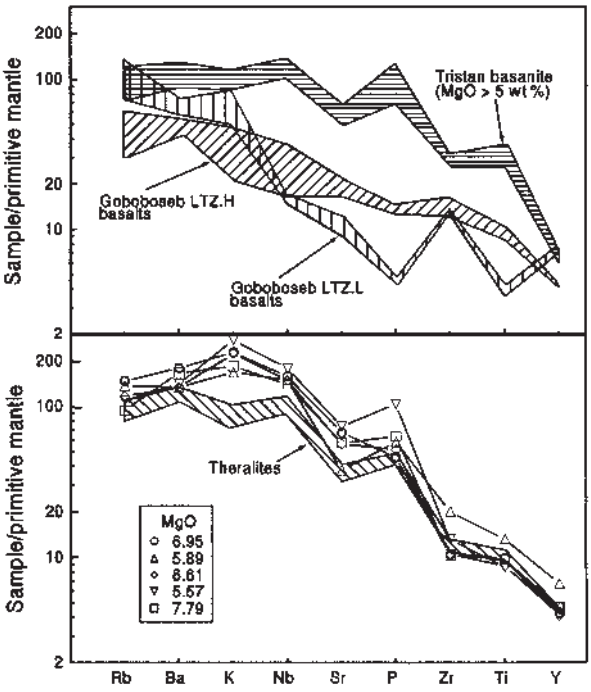

Fig. 15. Primitive mantle-normalized spidergram for Messum basanites having SiO_2 > 5 wt % [normalizing factors from Sun & McDonough (1989)]. Also shown is the spread of data for the theralites, the most mafic Goboboseb LTZ.H [Tafelkop magma type of Milner & le Roex (1996)] and LTZ.L basalts reported by Ewart *et al.* (1998*a*) and basanites from Tristan da Cunha (le Roex *et al.*, 1990).

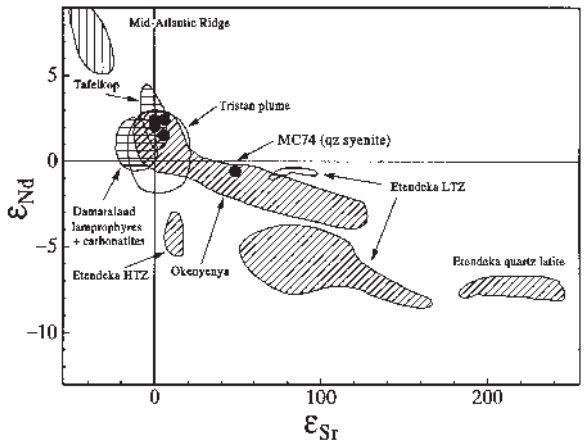

Fig. 16. ε_{Nd} vs ε_{Sr} calculated assuming an age of 128 Ma for Messum core samples [the average of the ^{40}Ar–^{39}Ar age of Renne *et al.* (1996) and the Rb–Sr age of Milner *et al.* (1995*b*)]. Also shown for comparison is the approximate field inferred for the Tristan plume at the same time (le Roex & Lanyon, 1998). The range of data for the Damaraland carbonatites is from le Roex & Lanyon (1998), Tafelkop (LTZ.H) and Okenyenya are from Milner & le Roex (1996), and the various Etendeka magma types from Ewart *et al.* (1998*a*, 1998*b*).

CONCLUSIONS

(1) The igneous rocks exposed in the core of the complex consist of an early formed subalkaline suite that shows a wide range of compositions including rock types compositionally similar to the quartz latite units erupted from Messum. The development of the alkaline core post-dated the formation of the sub-alkaline suite, and the

quartz latites were therefore probably erupted from Messum between the time of formation of the outer gabbroic sheets and intrusion of the alkaline core.

(2) The earliest alkaline intrusions were quartz syenites associated with minor more di erentiated granites. These rocks were later intruded by a series of slightly less di erentiated quartz microsyenite sheets.

(3) Two compositionally overlapping sub-suites of nepheline syenite intruded the quartz syenites that occupy the inner core. The earlier sub-suite assimilated quartz syenite during the fractionation process, whereas the later sub-suite evolved by closed system crystal fractionation.

(4) The alkaline intrusions of the core become progressively less contaminated with time. We favour a model where crystallization of each magma type against the walls of the conduit and/or magma chamber prevented contact between the subsequent magma and the contaminant. The quartz syenites were produced by contamination of a mantle-derived(?) magma by country rock or earlier formed quartz latite; the first nepheline syenites were contaminated by the quartz syenites and the later nepheline syenites were essentially uncontaminated.

(5) Trace element and Nd- and Sr-isotope composition of the basanite dykes, which are the youngest phase of intrusion at Messum, suggest that the Tristan plume is the ultimate source of alkaline magma in the Messum core. This hypothesis needs to be tested further by detailed isotope and trace element studies.

ACKNOWLEDGEMENTS

We are grateful to Andy Duncan and Protea Herschel for assistance in the field, and to the Geological Survey of Namibia for logistic support. Steve Richardson and Shireen Govender are thanked for producing the Sr- and Nd-isotope analyses, and Andreas Späth and Anton le Roex are thanked for providing the REE data. Financial support for the analytical work was provided by the Geological Survey of Namibia and the FRD. This paper was completed while the first author was on sabbatical leave at Monash University. Alan White is thanked for an informal review of an earlier version of the manuscript, and Elizabeth Dunworth and Bernard Bonin are thanked for their constructive comments on the submitted version.

REFERENCES

Deer, W. A., Howie, R. A. & Zussman, J. (1978). *Rock-forming Minerals, Volume 2A, Single Chain Silicates*. London: Longman, 668 pp.

DePaolo, D. (1981). Trace element and isotopic e ects of combined wall rock assimilation and fractional crystallization. *Earth and Planetary Science Letters* **53,** 189–202.

Droop, G. T. R. (1987). A general equation for estimating Fe^{3+} concentrations in ferromagnesian silicates and oxides from microprobe analyses using stoichiometric criteria. *Mineralogical Magazine* **51,** 431–435.

Duncan, A. R., Erlank, A. J. & Betton, P. J. (1984). Appendix 1: analytical techniques and data base descriptions. *Special Publication, Geological Society of South Africa* **13,** 389–395.

Dunworth, E. A. & Wilson, M. (1998). Olivine melilitites of the SW German Tertiary Volcanic Province: mineralogy and petrogenesis. *Journal of Petrology* **39,** 1805–1836.

Ewart, A., Milner, S. C., Armstrong, R. A. & Duncan, A. R. (1998*a*). Etendeka volcanism of the Goboboseb Mountains and Messum igneous complex, Namibia. Part I: Geochemical evidence of early Cretaceous Tristan plume melts and the role of crustal contamination in the Paraná–Etendeka CFB. *Journal of Petrology* **39,** 191–225.

Ewart, A., Milner, S. C., Armstrong, R. A. & Duncan, A. R. (1998*b*). Etendeka volcanism of the Goboboseb Mountains and Messum igneous complex, Namibia. Part II: Voluminous quartz latite volcanism of the Awahab magma system. *Journal of Petrology* **39,** 227–253.

Foland, K. A., Landoll, J. D., Henderson, C. M. B. & Jiangfeng, C. (1993). Formation of cogenetic quartz and nepheline syenites. *Geochimica et Cosmochimica Acta* **57,** 697–704.

Harris, C. (1995). Oxygen isotope geochemistry of the Mesozoic anorogenic complexes of Damaraland, northwest Namibia: evidence for crustal contamination and its e ect on silica saturation. *Contributions to Mineralogy and Petrology* **122,** 308–321.

Korn, H. & Martin, H. (1954). The Messum igneous complex in South West Africa. *Transactions of the Geological Society of South Africa* **57,** 83–124.

Leake, B. E. & 21 others (1997). Nomenclature of amphiboles: report of the Subcommittee on Amphiboles of the International Mineralogical Association Commission on New Minerals and Mineral Names. *Mineralogical Magazine* **61,** 295–321.

Le Bas, M. J. (1962). The role of aluminium in igneous clinopyroxenes with relation to their parentage. *American Journal of Science* **260,** 267–288.

Le Maitre, R. W. & 11 others (1989). *A Classification of Igneous Rocks and Glossary of Terms*. Oxford: Blackwell, 193 pp.

le Roex, A. P. (1985). Geochemistry, mineralogy and magmatic evolution of the basaltic and trachytic lavas from Gough Island, South Atlantic. *Journal of Petrology* **26,** 149–186.

le Roex, A. P. & Lanyon, R. (1998). Isotope and trace element geochemistry of Cretaceous Damaraland lamprophyres and carbonatites, northwestern Namibia: evidence for plume–lithosphere interactions. *Journal of Petrology* **39,** 1117–1146.

le Roex, A. P., Cli , R. A. & Adair, B. J. I. (1990). Tristan da Cunha, South Atlantic: geochemistry and petrogenesis of a basanite–phonolite lava series. *Journal of Petrology* **31,** 779–812.

Marsh, J. S. (1973). Relationships between transform directions and alkaline igneous rock lineaments in Africa and South America. *Earth and Planetary Science Letters* **18,** 317–323.

Martin, H., Mathias, M. & Simpson, E. S. W. (1960). The Damaraland sub-volcanic ring complexes in South West Africa. *International Geological Congress Reports, 21st Session, Norden* **13,** 156–174.

Martinez, I. A., Harris, C., le Roex, A. P. & Milner, S. C. (1996). Oxygen isotope evidence for extensive crustal contamination in the Okenyenya igneous complex, Namibia. *Geochimica et Cosmochimica Acta* **60,** 4497–4508.

Mathias, M. (1956). The petrology of the Messum Igneous Complex, South-West Africa. *Transactions of the Geological Society of South Africa* **59,** 23–57.

Mathias, M. (1957). The geochemistry of the Messum Igneous Complex, South-West Africa. *Geochimica et Cosmochimica Acta* **12,** 29–46.

Milner, S. C. & Ewart, A. (1989). The geology of the Goboboseb Mountain volcanics and their relationship to the Messum complex. *Communications of the Geological Survey of Namibia* **5,** 31–40.

Milner, S. C. & le Roex, A. P. (1996). Isotope characteristics of the Okenyenya igneous complex, northwestern Namibia: constraints on the composition of the early Tristan plume and the origin of the EM1 mantle component. *Earth and Planetary Science Letters* **141,** 277–291.

Milner, S. C., Duncan, A. R., Whittingham, A. M. & Ewart, A. (1995*a*). Trans-Atlantic correlation of erupted sequences and individual silicic volcanic units within the Paraná–Etendeka igneous province. *Journal of Volcanology and Geothermal Research* **69,** 137–157.

Milner, S. C., le Roex, A. P. & O'Connor, J. M. (1995*b*). Age of Mesozoic igneous rocks in northwest Namibia, and their relationship to continental breakup. *Journal of the Geological Society, London* **151,** 97–104.

Piranjo, F. (1994). Mineral resources of anorogenic alkaline complexes in Namibia: a review. *Australian Journal of Earth Sciences* **41,** 157–168.

Renne, P. R., Glen, J. M., Milner, S. C. & Duncan, A. R. (1996). Age of Etendeka flood volcanism and associated intrusions in southwestern Africa. *Geology* **24,** 659–662.

Rhodes, R. C. (1971). Structural geometry of sub-volcanic ring complexes as related to pre-Cenozoic motions of continental plates. *Tectonophysics* **12,** 111–117.

Schairer, J. F. (1950) The alkali feldspar join in the system $NaAlSiO_4$–$KAlSiO_4$–SiO_2. *Journal of Geology* **58,** 512.

Sheppard, S. M. F. & Harris, C. (1985). Hydrogen and oxygen isotope geochemistry of Ascension Island lavas and granites: variation with crystal fractionation and interaction with seawater. *Contributions to Mineralogy and Petrology* **91,** 74–81.

Siedner, G. & Miller, J. A. (1968). K–Ar age determinations on basaltic rocks from South West Africa, and their bearing on continental drift. *Earth and Planetary Science Letters* **4,** 451–458.

Smyth, J. R. (1980). Cation vacancies and the crystal chemistry of breakdown reactions in kimberlitic omphacites. *American Mineralogist* **65,** 1185–1191.

Sun, S.-S. & McDonough, W. F. (1989). Chemical and isotopic systematics of oceanic basalts: implications for mantle composition and process. In: Saunders, A. D. & Norry, M. J. (eds) *Magmatism in the Ocean Basins. Geological Society, London, Special Publication* **42,** 313–345.

Taylor, H. P., Jr & Sheppard, S. M. F. (1986). Igneous rocks: I. Processes of isotopic fractionation and isotope systematics. In: Valley, J. W., Taylor, H. P., Jr & O'Neil, J. R. (eds) *Stable Isotopes in High Temperature Geological Processes. Mineralogical Society of America, Reviews in Mineralogy* **16,** 227–271.

White, R. & Mackenzie, D. (1989). Magmatism at rift zones: the generation of volcanic continental margins and flood basalts. *Journal of Geophysical Research* **94,** 7685–7729.